High-Energy Astrophysical Neutrinos

Francis Halzen
Wisconsin IceCube Particle Physics Center
UW–Madison, Madison, WI USA
halzen@icecube.wisc.edu

November 9, 2016

Abstract

Chargeless, weakly-interacting neutrinos are ideal astronomical messengers because they travel through space without scattering, absorption, or deflection. They provide the only unobstructed view of cosmic accelerators. But this weak interaction also makes them notoriously difficult to detect, leading to neutrino observatories requiring large-scale detectors. The IceCube experiment discovered PeV-energy neutrinos originating beyond the Sun, with energies bracketed by those of TeV-energy gamma rays and EeV-energy extragalactic cosmic rays. In this chapter, we discuss the IceCube neutrino telescope, the status of the observation of cosmic neutrinos, and what neutrinos can tell us about the nonthermal Universe. Besides the search for the sources of Galactic and extragalactic cosmic rays, the scientific missions of IceCube and similar instruments under construction in the Mediterranean Sea and Lake Baikal include the observation of Galactic supernova explosions, the search for dark matter, and the study of neutrinos themselves.

1 Neutrino Astronomy: a Brief History

Soon after the 1956 observation of the neutrino [1], the idea emerged that it represented the ideal astronomical messenger. Neutrinos travel from the edge of the Universe without absorption and with no deflection by magnetic fields. Having essentially no mass and no electric charge, the neutrino is similar to the photon, except for one important attribute: its interactions with matter are extremely feeble. So, high-energy neutrinos may reach us unscathed from cosmic distances: from the inner neighborhood of black holes and from the nuclear furnaces where cosmic rays are born. But, their weak interactions also make cosmic neutrinos very difficult to detect. Immense particle detectors are required to collect cosmic neutrinos in statistically significant numbers [2]. By the 1970s, it was clear that a cubic-kilometer detector was needed to observe cosmic neutrinos produced in the interactions of cosmic rays with background

microwave photons [3]. Subsequent estimates for observing potential cosmic accelerators such as Galactic supernova remnants and gamma-ray bursts unfortunately pointed to the same exigent requirement [4, 5, 6]. Building a neutrino telescope has been a daunting technical challenge.

Given the detector's required size, early efforts concentrated on transforming large volumes of natural water into Cherenkov detectors that collect the light produced when neutrinos interact with nuclei in or near the detector [7]. After a two-decade-long effort, building the Deep Underwater Muon and Neutrino Detector (DUMAND) in the sea off the main island of Hawaii unfortunately failed [8]. However, DUMAND paved the way for later efforts by pioneering many of the detector technologies in use today, and by inspiring the deployment of a smaller instrument in Lake Baikal [9] as well as efforts to commission neutrino telescopes in the Mediterranean [10, 11, 12]. These efforts in turn have led towards the construction of KM3NeT. But the first telescope on the scale envisaged by the DUMAND collaboration was realized instead by transforming a large volume of transparent natural Antarctic ice into a particle detector, the Antarctic Muon and Neutrino Detector Array (AMANDA). In operation beginning in 2000, it represented a proof of concept for the kilometer-scale neutrino observatory, IceCube [13, 14].

Neutrino astronomy has achieved spectacular successes in the past: neutrino detectors have "seen" the Sun and detected a supernova in the Large Magellanic Cloud in 1987. Both observations were of tremendous importance; the former showed that neutrinos have mass, opening the first crack in the Standard Model of particle physics, and the latter confirmed the basic nuclear physics of the death of stars. Fig. 1 illustrates the neutrino energy spectrum covering an enormous range, from microwave energies (10^{-12} eV) to 10^{20} eV [15]. The figure is a mixture of observations and theoretical predictions. At low energy, the neutrino sky is dominated by neutrinos produced in the Big Bang. At MeV energy, neutrinos are produced by supernova explosions; the flux from the 1987 event is shown. At yet higher energies, the figure displays the measured atmospheric-neutrino flux, up to energies of 100 TeV by the AMANDA experiment [16]. Atmospheric neutrinos are a main player in our story, because they are the dominant background for extraterrestrial searches. The flux of atmospheric neutrinos falls dramatically with increasing energy; events above 100 TeV are rare, leaving a clear field of view for extraterrestrial sources.

The highest energy neutrinos in Fig. 1 are the decay products of pions produced by the interactions of cosmic rays with microwave photons [18]. Above a threshold of $\sim 4 \times 10^{19}$ eV, cosmic rays interact with the microwave background introducing an absorption feature in the cosmic-ray flux, the Greisen-Zatsepin-Kuzmin (GZK) cutoff. As a consequence, the mean free path of extragalactic cosmic rays propagating in the microwave background is limited to roughly 75 megaparsecs, and, therefore, the secondary neutrinos are the only probe of the still enigmatic sources at longer distances. What they will reveal is a matter of speculation. The calculation of the neutrino flux associated with the observed flux of extragalactic cosmic rays is straightforward and yields one event per year in a kilometer-scale detector. The flux, labeled GZK in Fig. 1, shares

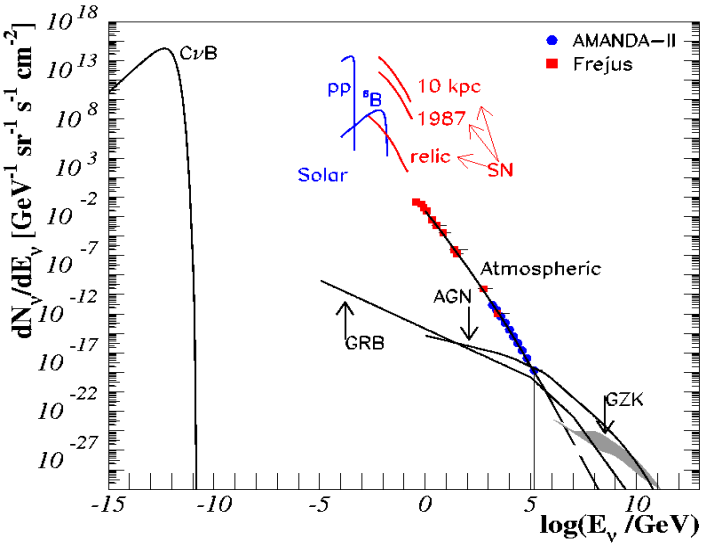

Figure 1: The cosmic-neutrino spectrum. Sources are the Big Bang (CνB), the Sun, supernovae (SN), atmospheric neutrinos, active galactic nuclei (AGN) galaxies, and GZK neutrinos. The data points are from detectors at the Frejus underground laboratory [17] (red) and from AMANDA [16] (blue).

the high-energy neutrino sky with neutrinos anticipated from gamma-ray bursts and active galactic nuclei [4, 5, 6].

A population of cosmic neutrinos covering the 30 TeV–1 PeV energy region were revealed by the first two years of IceCube data. Association of cosmic neutrinos with these, or any other source candidates, is still a work in progress. The goal of this chapter is to discuss these topics in some detail. Subsequently, it will briefly cover other uses of neutrino telescopes.

2 Rationale for the Construction of Kilometer-Scale Neutrino Detectors

The construction of kilometer-scale neutrino detectors was primarily motivated by the prospect of detecting neutrinos associated with the sources of high-energy cosmic rays. Cosmic accelerators produce particles with energies in excess of

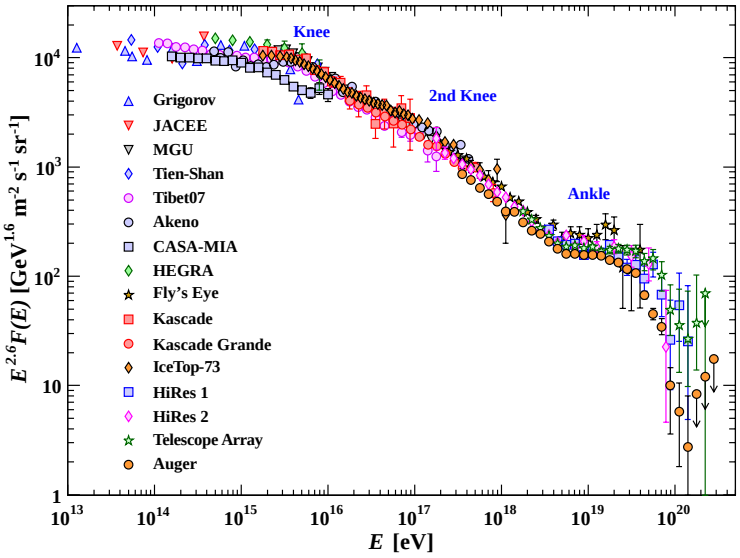

Figure 2: At the energies of interest here, the cosmic-ray spectrum follows a sequence of three power laws. The first two are separated by the "knee," the second and third by the "ankle." Cosmic rays beyond the ankle are a new population of particles produced in extragalactic sources. Note that the spectrum $F(E)(= dN/dE)$ has been multiplied by a power $E^{2.7}$ in order to visually enhance the structure in the spectrum (data compiled by Particle Data Group [20]).

100 EeV; we still do not know where or how [19]; see Fig. 2[1]. The bulk of the cosmic rays are Galactic in origin. Any association with our Galaxy presumably disappears at EeV energy when the gyroradius of a proton in the Galactic magnetic field exceeds its size. The cosmic-ray spectrum exhibits a rich structure above an energy of ~ 0.1 EeV, but where exactly the transition to extragalactic cosmic rays occurs is a matter of debate.

2.1 Cosmic-Ray Accelerators

The detailed blueprint for a cosmic-ray accelerator must meet two challenges: the highest-energy particles in the beam must reach energies beyond 10^3 TeV (10^8 TeV) for Galactic (extragalactic) sources and their luminosities must accommodate the observed flux. Both requirements represent severe constraints that have guided theoretical speculations. Acceleration of protons (or nuclei) to TeV energy and above requires massive bulk flows of relativistic charged particles. The blueprint of the accelerator can be copied from solar flares where

[1] We will use energy units TeV, PeV and EeV, increasing by factors of 1000 from GeV energy.

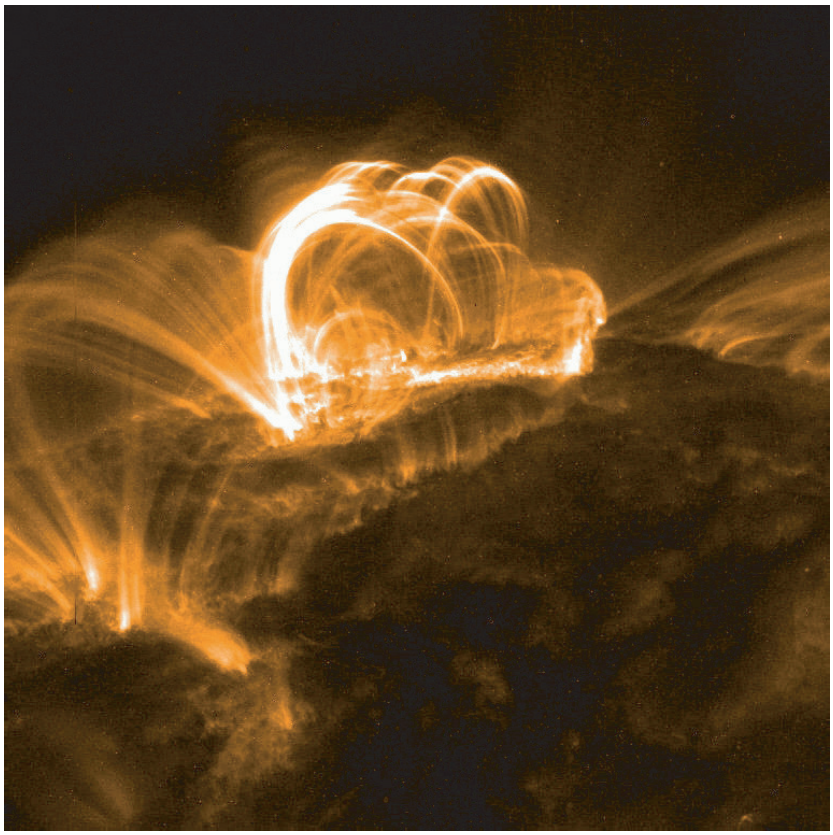

Figure 3: Opportunities exist near intense charged particle flows, seen as filaments in this X-ray picture of a solar flare, for solar particles to accelerate to GeV energy.

particles are accelerated to GeV energy by shocks and, possibly, reconnection; see Fig. 3. Recalling the Hillas formula that states that the gyroradius of the accelerated particle must be contained within the accelerating B-field region, $E/ZecB \leq R$, or

$$E \leq Ze\,c\,B\,R, \tag{1}$$

reaching GeV energy in solar flares is dimensionally impossible. In a solar flare, the extent R of the accelerating region and the magnitude of the magnetic fields B are not large enough to accelerate particles of charge Ze to energies beyond GeV; their velocity is taken to be the speed of light, c. The leading idea for accommodating the higher energies of the Galactic and extragalactic cosmic rays observed is that a fraction of the gravitational energy released in a stellar collapse is converted into particle acceleration, presumably by shocks.

Baade and Zwicky [21] suggested as early as 1934 that supernova remnants

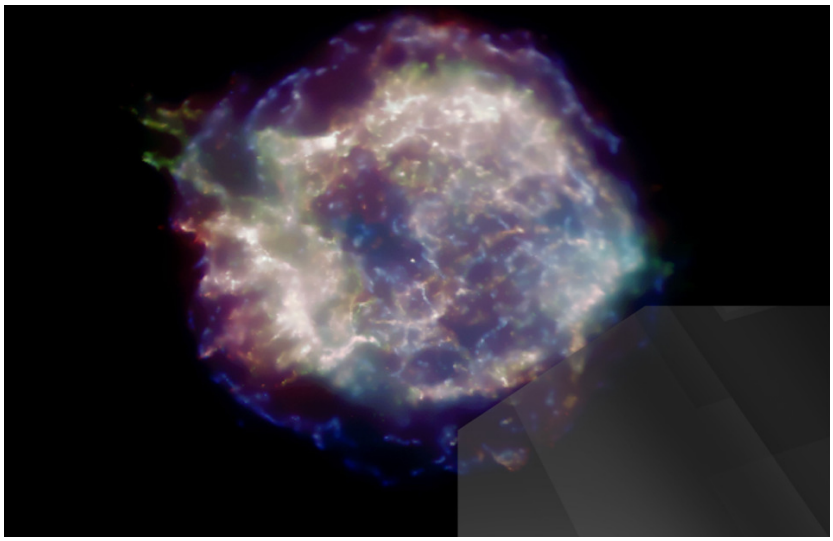

Figure 4: This X-ray picture of the supernova remnant CasA reveals strong particle flows near its periphery. We believe they are the site for accelerating Galactic cosmic rays to energies reaching the "knee" in the spectrum.

could be sources of the Galactic cosmic rays. It is assumed that, after the collapse, $\sim 10^{51}$ erg of energy is transformed into particle acceleration by diffusive shocks associated with young (~ 1000 year old) supernova remnants expanding into the interstellar medium. Like a snowplow, the shock sweeps up the $\sim 1\,\mathrm{proton/cm^3}$ density of hydrogen in the Galactic plane. The accumulation of dense filaments of particles in the outer reaches of the shock, clearly visible as sources of intense X-ray emission, are the sites of high magnetic fields; see Fig. 4. It is theorized that particles crossing these structures multiple times can be accelerated to high energies following an approximate power-law spectrum $dN/dE \sim E^{-2}$. The mechanism copies solar flares where filaments of high magnetic fields, visible in Fig. 3, are the sites for accelerating nuclear particles to tens of GeV. The higher energies reached in supernova remnants are the consequence of particle flows of much larger intensity powered by the gravitational energy released in the stellar collapse.

This idea has been widely accepted despite the fact that to date no source has been conclusively identified, neither by cosmic rays nor by accompanying gamma rays and neutrinos produced when the cosmic rays interact with Galactic hydrogen. Galactic cosmic rays reach energies of at least several PeV, the "knee" in the spectrum; therefore, their interactions should generate gamma rays and neutrinos from the decay of secondary pions reaching hundreds of TeV. Such sources, referred to as PeVatrons, have not been found; see, however, Ref. [22]. Nevertheless, Zwicky's suggestion has become the stuff of textbooks, and the reason is energetics: Three Galactic supernova explosions per century converting

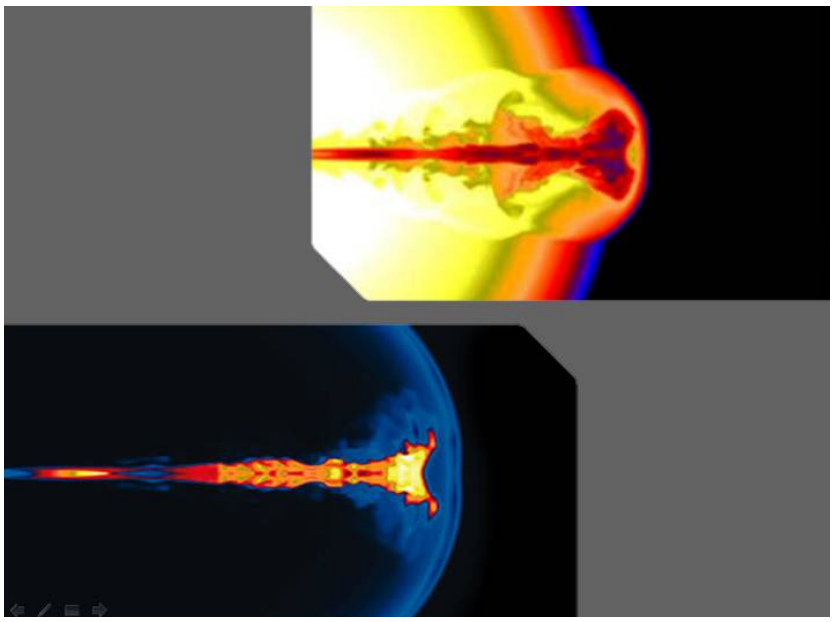

Figure 5: Colliding shocks in the simulation of a gamma-ray burst (GRB) fireball may accelerate cosmic rays to the highest energies observed. The filaments in the particle flow are directed along the rotation axis of the black hole. Animated view at http://www.nasa.gov/centers/goddard/news/topstory/2003/0618rosettaburst.html.

a reasonable fraction of a solar mass into particle acceleration can accommodate the steady flux of cosmic rays in the Galaxy. It is interesting to note that they originally assumed that the sources were extragalactic since the most recent supernova in the Milky Way was in 1572. After diffusion in the interstellar medium was understood, supernova explosions in the Milky Way became the source of choice for the origin of Galactic cosmic rays [23], although after more than 50 years the issue is still debated [24].

Energetics also guides speculations on the origin of extragalactic cosmic rays. By integrating the cosmic-ray spectrum above the ankle at $\sim 4\,\mathrm{EeV}$, it is possible to estimate [25] the energy density in extragalactic cosmic rays as $\sim 3 \times 10^{-19}\,\mathrm{erg\ cm^{-3}}$. This value is rather uncertain because of our ignorance of the energy where the transition from Galactic to extragalactic sources occurs. The power required for a population of sources to generate this energy density over the Hubble time of 10^{10} years is 2×10^{37} erg s^{-1} per Mpc^3. Long-duration gamma-ray bursts have been associated with the collapse of massive stars to black holes, and not to neutron stars, as is the case in a collapse powering a supernova remnant. A gamma-ray-burst fireball converts a fraction of a solar mass into the acceleration of electrons, seen as synchrotron photons. The observed energy in extragalactic cosmic rays can be accommodated with the reasonable assumption that shocks in the expanding gamma-ray burst (GRB) fireball convert roughly equal energy into the acceleration of electrons and cosmic rays [26]. It so happens that $2 \times 10^{51}\,\mathrm{erg}$ per GRB will yield the observed energy density in cosmic rays after 10^{10} years, given that their rate is on the order of 300 per Gpc^3 per year. Hundreds of bursts per year over a Hubble time produce the observed cosmic-ray density, just as three supernovae per century accommodate the steady flux in the Galaxy.

Problem solved? Not really: it turns out that the same result can be achieved assuming that active galactic nuclei convert, on average, 2×10^{44} erg s^{-1} each into particle acceleration [15]. This is an amount that matches their output in electromagnetic radiation. We will return to this point further on.

2.2 Neutrinos Associated with Cosmic Rays

Neutrinos will be produced at some level in association with the cosmic-ray beam. Cosmic rays accelerated in regions of high magnetic fields near black holes or neutron stars inevitably interact with radiation surrounding them. Thus, cosmic-ray accelerators are also "beam dumps" producing neutrino beams. The method is what is used for the production of neutrino beams at accelerator laboratories: the beam is dumped in a dense target where it produces pions and kaons that decay into neutrinos. All particles are absorbed in the extended target except for the neutrinos. Cosmic rays accelerated in supernova shocks interact with gas in the Galactic disk, producing equal numbers of pions of all three charges that decay into pionic photons and neutrinos. A larger source of secondaries is likely to be gas near the sources, for example cosmic rays interacting with high-density molecular clouds that are ubiquitous in the star-forming regions where supernovae are more likely to explode. For extragalactic

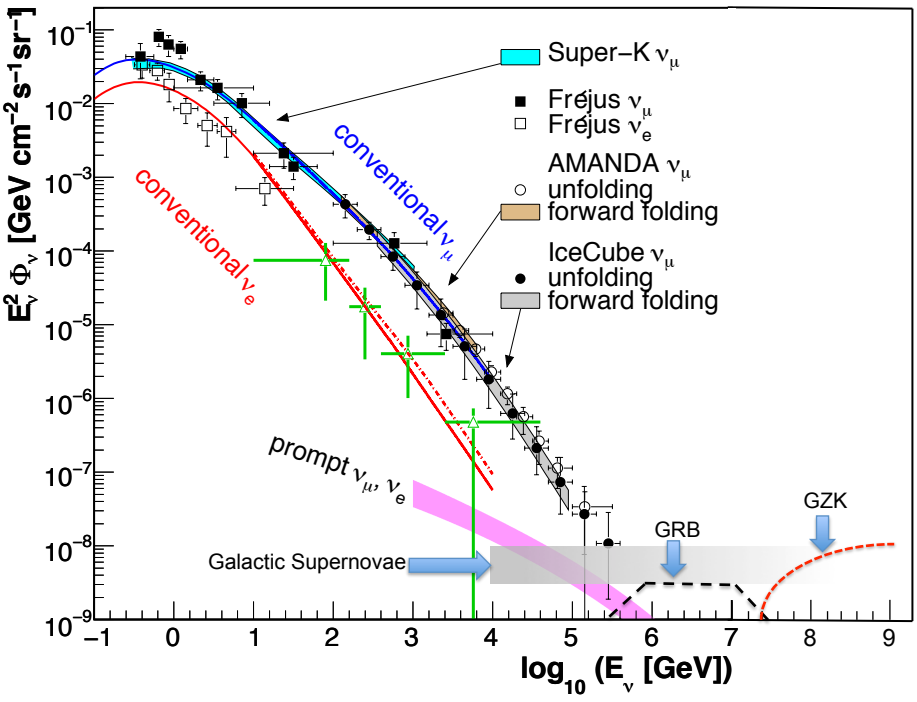

Figure 6: Anticipated astrophysical neutrino fluxes compared with measured and calculated fluxes of atmospheric neutrinos. Measurements of ν_μ from Super-K [27], Frejus [28], AMANDA, [29, 30] and IceCube [31, 32] are shown along with the electron-neutrino spectrum at high energy from Ref. [33] (green open triangles). Calculations of conventional ν_e (red line) and ν_μ (blue line) from Honda et al. [34], ν_e (red dotted line) from Bartol, [35] and charm-induced neutrinos (magenta band) [36] are also shown.

sources, the neutrino-producing target may be electromagnetic, for instance photons radiated by the accretion disk of an AGN, or synchrotron photons that coexist with protons in the expanding fireball producing a GRB. In Fig. 6, estimates of astrophysical neutrino fluxes are compared with measurements of atmospheric neutrinos. The shaded band indicates the level of model-dependent expectations for high-energy neutrinos of astrophysical origin. The estimates that we will discuss in more detail further on optimistically predicted a neutrino flux at a level of

$$E_\nu^2\,\mathrm{d}N_\nu/\mathrm{d}E_\nu \simeq 10^{-8}\,\mathrm{GeV\,cm^{-2}s^{-1}sr^{-1}} \qquad (2)$$

per flavor and formed the rational for building a kilometer-scale detector; this is indeed the magnitude of the cosmic component of the neutrino spectrum above 100 TeV revealed by IceCube'sdata.

How many neutrinos and, inevitably, gamma rays are produced in association with the cosmic-ray beam? Generically, a cosmic-ray source should also be a beam dump. Cosmic rays accelerated in regions of high magnetic fields near black holes may interact with radiation surrounding them, e.g., UV photons in some active galaxies or MeV photons in GRB fireballs. In these interactions, neutral and charged pion secondaries are produced by the processes

$$p + \gamma \to \Delta^+ \to \pi^0 + p \;\; \text{and} \;\; p + \gamma \to \Delta^+ \to \pi^+ + n. \tag{3}$$

While secondary protons may remain trapped and lose energy in the high magnetic fields, neutrons and the decay products of neutral and charged pions escape with high energy. The energy escaping the source is therefore distributed among cosmic rays, gamma rays and neutrinos, particles produced by the decay of neutrons, neutral pions and charged pions, respectively.

Galactic supernova shocks are in contrast an example of a hadronic beam dump. Cosmic rays mostly interact with the hydrogen in the Galactic disk, producing equal numbers of pions of all three charges in hadronic collisions $p + p \to n\,[\,\pi^0 + \pi^+ + \pi^-] + X$; n is the pion multiplicity.

In a generic cosmic beam dump, accelerated cosmic rays, assumed to be protons for illustration, interact with a photon target. These may be photons radiated by the accretion disk in AGNs and synchrotron photons that co-exist with protons in the exploding fireball producing a GRB. Their interactions produce charged and neutral pions according to Eq. 3, with probabilities of 2/3 and 1/3, respectively. Subsequently, the pions decay into gamma rays and neutrinos that carry, on average, 1/2 and 1/4 of the energy of the parent pion. We further assume that, on average, the four leptons in the decay $\pi^+ \to \nu_\mu + \mu^+ \to \nu_\mu + (e^+ + \nu_e + \bar{\nu}_\mu)$ equally share the charged pion's energy. The energy of the pionic leptons relative to the proton is:

$$x_\nu = \frac{E_\nu}{E_p} = \frac{1}{4}\langle x_{p\to\pi}\rangle \;\simeq\; \frac{1}{20} \tag{4}$$

and

$$x_\gamma = \frac{E_\gamma}{E_p} = \frac{1}{2}\langle x_{p\to\pi}\rangle \;\simeq\; \frac{1}{10}. \tag{5}$$

Here,

$$\langle x_{p\to\pi}\rangle \;=\; \langle\frac{E_\pi}{E_p}\rangle \;\simeq\; 0.2 \tag{6}$$

is the average energy transferred from the proton to the pion.

While both gamma-ray and neutrino fluxes can be calculated knowing the density of the accelerated protons and the density of the target material, their relative flux is independent of the details of the production mechanism. The spectral production rates $\mathrm{d}N/\mathrm{d}E\mathrm{d}t$ of neutrinos and gamma rays are related by

$$\frac{1}{3}\sum_{\nu_\alpha} E_\nu^2 \frac{\mathrm{d}N_\nu}{\mathrm{d}E_\nu \mathrm{d}t}(E_\nu) \simeq \frac{K_\pi}{4} E_\gamma^2 \frac{\mathrm{d}N_\gamma}{\mathrm{d}E_\gamma \mathrm{d}t}(E_\gamma)\,. \tag{7}$$

Here, N and E denote the number and energy of neutrinos and gamma rays and ν stands for the neutrino flavor. Note that this relation is solid and depends only on the charged-to-neutral secondary pion ratio, with $K_\pi = 1(2)$ for $\gamma(pp)$ neutrino-producing interactions. In deriving the relative number of neutrinos and gamma rays, one must be aware of the fact that the neutrino flux represents the sum of the neutrinos and antineutrinos, which cannot be separated by current experiments.

The production rate of gamma rays described by Eq. 7 is not necessarily the emission rate observed. For instance, in cosmic accelerators that efficiently produce neutrinos via $p\gamma$ interactions, the target photon field can also efficiently reduce the pionic gamma rays via pair production. This is a calorimetric process that will, however, conserve the total energy of hadronic gamma rays. The production of photons in association with cosmic neutrinos is inevitable. The relation is however calorimetric; unlike neutrinos, photons reach Earth after propagation in the universal microwave and infrared photon backgrounds to reach our telescopes with TeV energy, or below. Also, one must be aware of the fact that inverse-Compton scattering and synchrotron emission by accelerated electrons in magnetic fields in the source have the potential to produce gamma rays; not every high-energy gamma ray is pionic.

The estimates in Fig. 6 of the neutrino flux associated with cosmic rays accelerated in supernova remnants and GRBs are relatively straightforward as both the beam, identified with the observed cosmic-ray flux, and the targets, observed by astronomers, are known. In the case of supernova remnants, the main uncertainty is the availability of nearby target material. In the case of GRBs, the main uncertainty is the fraction of the extragalactic cosmic ray population that comes from this source. The ongoing search by IceCube for neutrinos in coincidence with and in the direction of GRB alerts issued by astronomical telescopes has limited the GRB neutrino flux to less that 1% of the diffuse cosmic neutrino flux actually observed by the experiment [37]. However, this may not conclusively rule out GRBs as a source of cosmic rays; the events that produce the spectacular photon displays catalogued by astronomers as GRBs may not be the stellar collapses that are sources of neutrinos. We will return to this point further on when we discuss acceleration of cosmic rays in GRB fireballs. Nevertheless, the failure of IceCube to observe neutrinos from GRBs has lately promoted AGNs as the best-bet source of the cosmic neutrinos observed.

Active galaxies are complex systems with many possible sites for accelerating cosmic rays and for targets to produce neutrinos. First, if acceleration occurs mainly at the spectacular termination shocks of the jets in intergalactic space [38], there would be little target material available and few neutrinos produced. In contrast, production of neutrinos near the black hole [39], or in collisions with interstellar matter of the accelerated particles diffusing in the magnetic field of the galaxy hosting the black hole [40], could yield fluxes at the level observed. We will work through these examples further on.

One generic picture in which the neutrino luminosity is directly related to the contribution of the sources to extragalactic cosmic rays arises if acceleration occurs in the jets of AGNs (or GRBs) [41, 42]. High-energy protons interact in

the intense radiation fields inside the jets. In the $p\gamma \to p\pi^0$ channel, the protons remain in the accelerator. In the $p\gamma \to n\pi^+$ channel, however, the neutrons escape and eventually decay to produce cosmic-ray protons, while the pions decay to neutrinos. The luminosity of neutrinos from photo-pion production is then directly related by kinematics to the cosmic-ray protons that come from decay of the escaping neutrons.

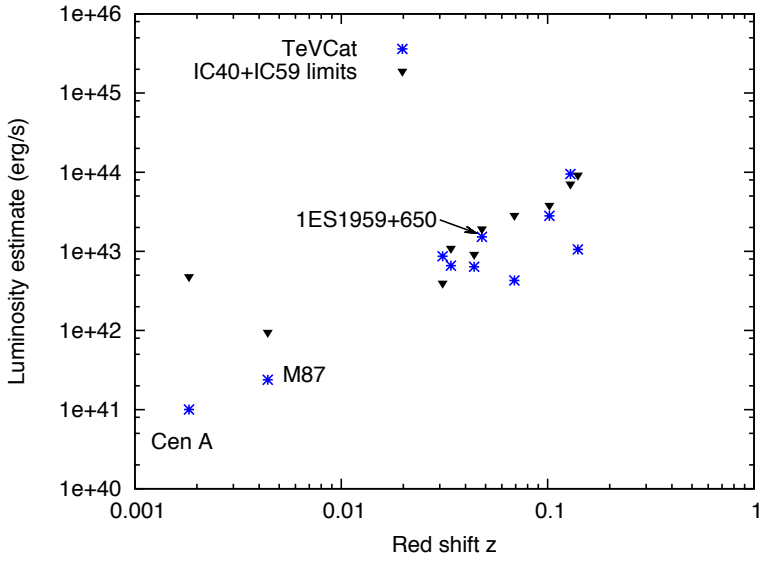

Figure 7: Limits on the neutrino flux from selected active galaxies derived from IceCube data taken during construction, when the instrument was operating with 40 and 59 strings of the total 86 instrumented strings of DOMs [43]. These are compared with the TeV photon flux for nearby AGNs. Note that energy units are in ergs, not TeV.

TeV gamma rays are measured from many AGN blazars [44]. Although the observed gamma rays are likely to be from accelerated electrons, which radiate more efficiently than protons, the gamma-ray luminosity may give an indication of the overall cosmic-ray luminosity and hence of the possible level of neutrino production [45, 46]. In this context, we introduce Fig. 7 [47] showing IceCube upper limits [43] on the neutrino flux from nearby AGNs as a function of their distance. The sources at red shifts between 0.03 and 0.2 are Northern Hemisphere blazars for which distances and intensities are listed in TeVCat [44] and for which IceCube also has upper limits. In several cases, the muon-neutrino limits have reached the level of the TeV photon flux. One can sum the sources shown in the figure into a diffuse flux. The result, after accounting for the

distances and luminosities, is $3 \times 10^{-9}\,\mathrm{GeV\,cm^{-2}\,s^{-1}\,sr^{-1}}$, or approximately $10^{-8}\,\mathrm{GeV\,cm^{-2}\,s^{-1}\,sr^{-1}}$ for all neutrino flavors. This is at the level of the generic astrophysical neutrino flux of Eq. 2. At this intensity, neutrinos from theorized cosmic-ray accelerators will cross the steeply falling atmospheric neutrino flux above an energy of $\sim 300\,\mathrm{TeV}$; see Fig. 6. The level of events observed in a cubic-kilometer neutrino detector is $10 \sim 100$ ν_μ-induced events per year. Such estimates reinforce the logic for building a cubic kilometer neutrino detector [48].

3 Cosmic Accelerators and Cosmic Beam Dumps: Estimates of the Neutrino Flux

We will discuss next two generic blueprints for beam dumps producing neutrinos in association with cosmic-ray accelerators: a beam interacting with nearby gas, radiation fields, or molecular clouds, and the relativistically expanding fireball following stellar collapse.

3.1 Extragalactic Neutrino-Producing Beam Dumps

An active galaxy presents multiple opportunities for accelerating particles in the in- and outflows associated with the supermassive black hole. The high energy particles may subsequently produce neutrinos in interactions with multiple targets such as the dense matter near the black hole, the galactic disk of the galaxy associated with the black hole, photons produced in the jet or radiated from the accretion disk. It is therefore useful to start by considering a generic beam dump where a beam of protons an initial flux $j_{\mathrm{p}}\left(E_{\mathrm{p}}\right)$ interacts with a target of density n over a distance l. The optical depth target after the proton travels a distance l' is given by:

$$\tau' = \frac{l'}{\lambda} = n l' \sigma_{pp}. \tag{8}$$

Each time a proton interacts it deposits $K_p E_p$ energy into $\langle n_\pi \rangle$ pions of average energy $\langle E_\pi \rangle$; here $K_p \simeq 0.2$ is the proton inelasticity. Energy conservation implies that

$$K_p E_p = E_\pi = \langle n_\pi \rangle \langle E_\pi \rangle . \tag{9}$$

The flux of pions produced per energy and time interval $q_{\pi^\pm}(E_\pi)$ is related to the proton interaction rate in the target $q_{\mathrm{p}}(E_{\mathrm{p}},\, \tau)$ by

$$q_{\pi^\pm} = \int_{E_{\mathrm{th}}}^{\infty} dE_p \int_0^l dl'\, q_p\left(E_p, \tau'\right)\, \delta\left(E_\pi - \langle E_\pi \rangle\right) , \tag{10}$$

where $q_p\left(E_p\,, \tau\right) = j_p\left(E_p\right) \exp(-\tau)$ and $j_p\left(E_p\right)$ the incident proton flux entering the target. The delta function expresses the fact that all pions are produced with the same average energy $\langle E_\pi \rangle$.

Typically, one makes the approximations that the proton cross section is independent of energy, $\sigma_{pp} \approx 3 \cdot 10^{-26}$ cm^2, and as a result

$$q_{\pi^\pm} = \int_{E_{\rm th}}^{\infty} dE_{\rm p} \left(1 - \exp(-\tau)\right) \, j_p(E_p) \, \delta \left(E_\pi - \langle E_\pi \rangle\right) \, . \tag{11}$$

Two limiting cases are often relevant. When all protons interact $(1 - \exp(-\tau)) \rightarrow 1$. In other cases, the optical depth is small and $(1 - \exp(-\tau)) \rightarrow \tau$, with $\tau \simeq l \, n \, \sigma_{pp}$,

$$q_{\pi^\pm} = n \, l \, \sigma_{pp} \int_{E_{\rm th}}^{\infty} dE_p \, j_p \left(E_p\right) \, \delta \left(E_\pi - \langle E_\pi \rangle\right) \, . \tag{12}$$

The integral can be performed by rewriting the delta function as

$$\delta \left(E_\pi - \frac{K_p}{\langle n_\pi \rangle} \, E_p \right) \, = \, \frac{\langle n_\pi \rangle}{K_p} \, \delta \left(E_p - \frac{\langle n_\pi \rangle \, \langle E_\pi \rangle}{K_p} \right) \tag{13}$$

using Eq. 9. We thus obtain the result that

$$q_{\pi^\pm} = n \, l \, \sigma_{pp} \, \langle n_\pi \rangle \, \frac{1}{f_\pi} \, j_p \left(E_p\right) \, , \tag{14}$$

with $f_\pi = K_p = E_\pi / E_p$, the fraction of the incident proton energy going into pions, using a more common notation. Note that in the case of a target where all protons interact, i.e. $(1 - \exp(-\tau)) \rightarrow 1$, we obtain the relations that reflect particle and energy conservation:

$$E_\pi \, q_{\pi^\pm} = \langle n_\pi \rangle \, E_p q_p \, , \tag{15}$$

and

$$E_\pi^2 \, q_{\pi^\pm} = K_p \, E_p^2 q_p \, .$$

For simple, yet more realistic, calculations we can follow Mannheim [49] who introduce the fact that the multiplicity of pions grows with the proton energy. Starting from a pair of pions $pp \rightarrow pp + \pi^+ \pi^-$ at threshold E_{th}, the multiplicity grows as

$$\langle n_\pi \rangle = 2 \left(\frac{E_p - E_{th}}{\rm GeV} \right)^{1/4} \, , \tag{17}$$

and

$$\langle E_\pi \rangle = \frac{1}{6} (E_{\rm p} - m_p c^2)^{3/4} \, {\rm GeV}. \tag{18}$$

The formalism introduced combined with these parametrization, allows us to reproduce the results of detailed simulations. Finally, given the number of protons produced by the accelerator per energy and time interval

$$j_p(E_p) = A_p \left(\frac{E_p - m_p c^2}{\rm GeV} \right)^{-\gamma} \, , \tag{19}$$

we obtain a pion rate *at the source*:

$$q_{\pi^\pm}(E_\pi) \approx 26\, n\, l\, A_p\, \sigma_{pp} \left(\frac{6E_\pi}{\mathrm{GeV}}\right)^{-\frac{4}{3}(\gamma-\frac{1}{2})} . \tag{20}$$

The total neutrino rate *at the source* is then given by the sum of the emissivities of the first muon neutrino, directly from the pion, and those of the second muon neutrino and the electron neutrino from the muon decay:

$$q_{\nu,\mathrm{tot}} = q^{(1)}_{\nu_\mu} + q^{(2)}_{\nu_\mu} + q_{\nu_e} . \tag{21}$$

As previously discussed, we will make the approximation that the total energy of the pions is distributed equally among the four decay leptons (see e.g., Ref. [50]),

$$q_{\nu_i}(E_{\nu_i}) = q_\pi(4E_{\nu_1})dE_\pi/dE_{\nu_i} = 4q_\pi(4E_{\nu_i}) \tag{22}$$

for each neutrino, $\nu_i = \overline{\nu}_e/\nu_e$, ν_μ, $\overline{\nu}_\mu$. As IceCube does not distinguish between neutrinos and antineutrinos, we will not separate neutrinos from antineutrinos. Another way of stating the approximation introduced is that the number of neutrinos produced per flavor in the energy bin dE_ν arises from the original pion in the energy bin $dE_\pi = 4dE_\nu$; therefore, $q_\nu(E_\nu)\, dE_\nu = q_\pi(4\, E_\nu)dE_\pi$.

The final result for the total neutrino emission rate at the source is given by

$$q_{\nu,\mathrm{tot}} \approx 3 \times 10^2 N A_\mathrm{p} \sigma_\mathrm{pp} \left(\frac{24E_\nu}{\mathrm{GeV}}\right)^{-\frac{4}{3}\gamma+\frac{2}{3}} . \tag{23}$$

Eq. 23 provides us with an estimate of the total neutrino flux at the source in terms of three key quantities: A_p and γ, the normalization and spectral slope of the flux of the accelerator, and the column density $N \sim ln$.

The spectral index is routinely taken to be $\gamma = 2$, a value obtained from diffusive shock acceleration and, in any case, typical of the spectral flux observed for the spectrum of gamma rays in nonthermal sources. The column density $N = ln$ is usually taken from astronomical information, with l being the distance that the cosmic rays travel through a photon target of density n. For instance, in the case of a galaxy, l could be the diffusion length of the cosmic rays in the magnetic field of the galaxy. This allows the protons to interact with a typical density of dust of $n = 1\,\mathrm{cm}^{-3}$ over an extended pathlength determined by the diffusion time. The typical diffusion distance before escape of the galaxy is given by

$$d_{diff} = 2\sqrt{D(E_\mathrm{p})\, t_{esc}}\,, \tag{24}$$

where D is the diffusion coefficient and t_{esc} is the escape time. In this case, the distance in the calculation is identified with $l = ct_{esc}$. Finally, the normalization of the cosmic-ray flux A_p is typically determined from the requirement that the source reproduce the cosmic flux observed at Earth [39, 40].

In the end, the flux of IceCube data can be described by this procedure with the reasonable assumptions that $p = 2$ and $l = 10\,\mathrm{kpc}$, typical of our own

Galaxy. Additionally, an extragalactic diffuse photon flux is obtained consistent with the Fermi measurements in the GeV-TeV energy range [40].

Alternatively, one may determine $A_{\rm p}$ for individual galaxies, determine their neutrino flux, and subsequently do the summation over all sources. An example can be found in Ref. [39] where the cosmic-ray flux is obtained from the following considerations: The radio luminosity of AGNs, L, provides a measure for the AGN luminosity in electrons. The electron luminosity is equal to or larger than the radio luminosity of the source, as the latter is produced when electrons are accelerated and emit synchrotron radiation: $L_{\rm e} = \chi L$ with $\chi \geq 1$. Hadronic cosmic rays and electrons are connected by a constant fraction f_e: $L_{\rm e} = f_e L_{\rm p}$, which is on the order of 0.1 [39]. With

$$L_{\rm p} = \int j_{\rm p}(E_{\rm p})\, d(E_{\rm p}) \approx \frac{\chi L}{f_e}\,, \tag{25}$$

the normalization of the CR spectrum is

$$A_{\rm p} = A_{\rm p}(L,z) = \frac{\chi}{f_e}\left[\ln\left(E_{\rm max}/E_{\rm min}\right)\right]^{-1} L\,{\rm GeV}^{-2} \tag{26}$$

for $\gamma = 2$; the generalization for $\gamma \neq 2$ is straightforward.

Finally, the diffuse neutrino flux at Earth is obtained from the single source flux of Eq. 23, the cosmic-ray spectrum normalized by Eq. 26, and

$$\Phi_\nu = \int_L \int_z \frac{q_{\nu,tot}}{4\,\pi\, d_L(z)^2} \frac{dn_{\rm AGN}}{dV\, dL} \frac{dV}{dz}\, dz\, dL\,. \tag{27}$$

Here, d_L is the luminosity distance, $dn_{\rm AGN}/(dV\, dL)$ is the radio luminosity function of the AGN, and dV/dz is the comoving volume at a fixed redshift z. The radio luminosity function is usually represented by the product of a luminosity-dependent and a redshift-dependent function, $dn_{\rm AGN}/(dV\, dL) = g(L)f(z)$. This framework for producing neutrinos in AGNs can accommodate the diffuse flux observed by IceCube; more details can be found in Ref. [39].The neutrino production happens in the relatively dense matter near the black hole, illustrating how two very different mechanisms manage to accommodate the IceCube result. The details may vary, but in general beam dumps producing similar energies in neutrinos, photons, and cosmic rays match the diffuse neutrino flux observed. We will return to this point when discussing the IceCube results.

In yet another scenario, Wang and Loeb argue that quasar driven outflows interact with interstellar protons to produce IceCube's neutrinos [51]. While the examples illustrate that AGNs are plausible sources of the neutrinos observed by IceCube, they do not have the power of proof given the presence of adjustable parameters. This does not mean that a conclusive association is impossible. AGNs are episodic sources that burst, increasing their flux by over one order of magnitude for periods of seconds to days, sometimes even years. A correlation of the arrival of IceCube neutrinos in coincidence with such bursts can provide a smoking gun for their origin; for a recent discussion, see Ref. [52].

3.2 Galactic Neutrino-Producing Beam Dumps

The rationale for kilometer-scale neutrino detectors is that their sensitivity is sufficient to reveal generic cosmic-ray sources with an energy density in neutrinos comparable to their energy density in cosmic rays [41] and pionic TeV gamma rays [45]. Interestingly, this condition may be satisfied by the sources of Galactic cosmic rays.

The energy density of the cosmic rays in our Galaxy is $\rho_E \sim 10^{-12}\,\mathrm{erg\,cm^{-3}}$. Galactic cosmic rays do not exist forever; they diffuse within microgauss fields and remain trapped for an average containment time of 3×10^6 years. The power needed to maintain a steady energy density requires accelerators delivering $10^{41}\,\mathrm{erg/s}$. This happens to be 10% of the power produced by supernovae releasing $10^{51}\,\mathrm{erg}$ every 30 years ($10^{51}\,\mathrm{erg}$ correspond to 1% of the binding energy of a neutron star after 99% is initially lost to neutrinos). This coincidence is the basis for the idea that shocks produced by supernovae exploding into the interstellar medium are the accelerators of Galactic cosmic rays.

A generic supernova remnant releasing an energy of $W \sim 10^{50}\,\mathrm{erg}$ into the acceleration of cosmic rays will inevitably generate TeV gamma rays by interacting with the hydrogen in the Galactic disk. The emissivity in pionic gamma rays is calculated using the formalism previously introduced for the calculation of the neutrino flux; see Eq. 12. Here every neutral pion in the dump produces two photons with half its energy. The emissivity Q_γ, the number of photons produced per unit volume and time, is simply proportional to the density of cosmic rays n_{cr} and to the target density n of hydrogen atoms. Here, $n_{cr} \simeq 4 \times 10^{-14}\,\mathrm{cm^{-3}}$ is obtained by integrating the proton spectrum for energies in excess of 1 TeV. Following the formalism introduced by Eq. 10–Eq. 12, we obtain the emissivity of gamma rays,

$$Q_\gamma(>1\,\mathrm{TeV}) \simeq c\,\frac{2}{f_\pi}\,\sigma_{pp}\,n\,n_{cr}(>1\,\mathrm{TeV}). \tag{28}$$

The production rate is defined per volume; the relation to q_π is $q = dN/dEdAdt = cdN/dEdAdl = cQ$, with $cdt = dl$ and $dAdl = dV$. Assuming an E^{-2} spectrum,

$$Q_\gamma(>1\,\mathrm{TeV}) \simeq 10^{-29}\,\left(\frac{n}{1\,\mathrm{cm^{-3}}}\right)\,\mathrm{cm^{-3}\,s^{-1}}\,. \tag{29}$$

The proportionality factor in Eq. 28 is determined by particle physics; x_γ is the average energy of secondary photons relative to the cosmic-ray protons, and $\lambda_{pp} = (n\sigma_{pp})^{-1}$ is the proton interaction length ($\sigma_{pp} \simeq 40\,\mathrm{mb}$) in a density n of hydrogen atoms. The corresponding luminosity is

$$L_\gamma(>1\,\mathrm{TeV}) \simeq Q_\gamma\,\frac{W}{\rho_E} \tag{30}$$

where W/ρ_E is the volume occupied by the supernova remnant; given the ambient density $\rho_E \sim 10^{-12}\,\mathrm{erg\,cm^{-3}}$ of Galactic cosmic rays [4], a supernova with energy $W \sim 10^{50}\,\mathrm{erg}$ in cosmic rays occupies the volume W/ρ_E. We here

made the approximation that the density of particles in the remnant is not very different from the ambient energy density.

We thus predict [53, 54] a rate of TeV photons from a supernova remnant at a nominal distance d on the order of 1 kpc of

$$\int_{E>1\mathrm{TeV}} \frac{dN_\gamma}{dE_\gamma} dE_\gamma = \frac{L_\gamma(>1\mathrm{TeV})}{4\pi d^2}$$
$$\simeq 10^{-12} - 10^{-11} \left(\frac{\mathrm{photons}}{\mathrm{cm}^2\,\mathrm{s}}\right) \left(\frac{W}{10^{50}\,\mathrm{erg}}\right) \left(\frac{n}{1\,\mathrm{cm}^{-3}}\right) \left(\frac{d}{1\,\mathrm{kpc}}\right)^{-2}. \quad (31)$$

As discussed in the introduction, the position of the knee in the cosmic ray spectrum indicates that some sources accelerate cosmic rays to energies of several PeV. These PeVatrons therefore produce pionic gamma rays whose spectrum can extend to several hundred TeV without cutting off. For such sources the gamma-ray flux in the TeV energy range can be parametrized in terms of a spectral slope α_γ, an energy $E_{cut,\gamma}$ where the accelerator cuts off, and a normalization k_γ:

$$\frac{dN_\gamma(E_\gamma)}{dE_\gamma} = k_\gamma \left(\frac{E_\gamma}{\mathrm{TeV}}\right)^{-\alpha_\gamma} \exp\left(-\sqrt{\frac{E_\gamma}{E_{cut,\gamma}}}\right). \quad (32)$$

The estimate in Eq. 31 indicates that fluxes as large as $dN_\gamma/dE_\gamma \sim 10^{-12}$–$10^{-14}$ (TeV^{-1} cm^{-2} s^{-1}) can be expected at energies of $\mathcal{O}$ (10 TeV).

We therefore concentrate on the search for PeVatrons, supernova remnants with the required energetics to produce cosmic rays, at least up to the knee in the spectrum. They may have been revealed by the highest energy all-sky survey in $\sim$ 10 TeV gamma rays using the Milagro detector [55]. A subset of sources, located within nearby star-forming regions in Cygnus and in the vicinity of Galactic latitude $l = 40$ degrees, are identified; some cannot be readily associated with known supernova remnants or with nonthermal sources observed at other wavelengths. Subsequently, directional air Cherenkov telescopes were pointed at three of the sources, revealing them as PeVatron candidates with an approximate E^{-2} energy spectrum that extends to tens of TeV without evidence for a cutoff [56], in contrast with the best studied supernova remnants RX J1713-3946 and RX J0852.0-4622 (Vela Junior).

Some Milagro sources may actually be molecular clouds illuminated by the cosmic-ray beam accelerated in young remnants located within $\sim$ 100 pc. Indeed, one expects that multi-PeV cosmic rays are accelerated only over a short time period when the shock velocity is high, i.e., when the remnant transitions from free expansion to the beginning of the Sedov phase. The high-energy particles can produce photons and neutrinos over much longer periods when they diffuse through the interstellar medium to interact with nearby molecular clouds [57]. An association of molecular clouds and supernova remnants is expected, of course, in star-forming regions. In this case, any confusion with synchrotron photons is unlikely.

Ground-based and satellite-borne instruments with improved sensitivity are able to conclusively pinpoint supernova remnants as the sources of cosmic-ray acceleration by identifying accompanying gamma rays of pion origin. The Fermi Large Area Telescope has detected pion-decay feature in the gamma-ray spectra of two supernova remnants, IC 443 and W44 [58]. In contrast, GeV gamma ray data from Fermi LAT have challenged the hadronic interpretation of the GeV-TeV radiation from one of the best-studied candidates, RX J1713-3946 [59]. The most promising PeVatron candidate to date is, instead, the center of the Galaxy, as reported by the HESS Collaboration, see Ref. [22]. Detecting the accompanying neutrinos from supernova remnants or the Galactic Centre would provide incontrovertible evidence for cosmic-ray acceleration.

Particle physics dictates the relation between pionic gamma rays and neutrinos and basically predicts the production of a $\nu_\mu + \bar{\nu}_\mu$ pair for every two gamma rays seen by Milagro. This calculation can be performed using the formalism discussed with approximately the same outcome. Operating the complete IceCube detector for several years should yield confirmation that some of the Milagro sources produce pionic gamma rays; see Fig. 8.

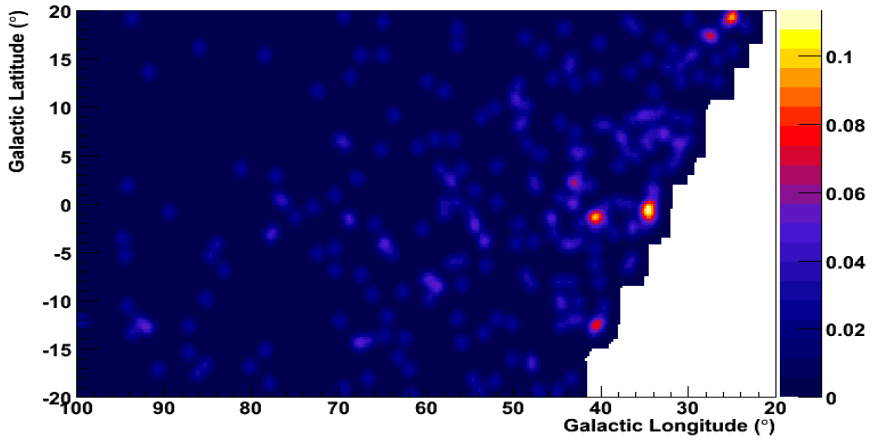

Figure 8: Simulated sky map of IceCube in Galactic coordinates after five years of operation of the completed detector. Two Milagro sources are visible with four events for MGRO J1852+01 and three events for MGRO J1908+06 with energy in excess of 40 TeV. These, as well as the background events, have been randomly distributed according to the resolution of the detector and the size of the sources.

The quantitative statistics can be summarized in the following. For average values of the parameters describing the flux, we find that the IceCube detector could confirm sources in the Milagro sky map as sites of cosmic-ray acceleration at the 3σ level in less than one year and at the 5σ level in three years [53]. We here assume that the source extends to 300 TeV, or 10% of the energy

of the cosmic rays near the knee in the spectrum. These results agree with previous estimates [60, 61]. There are intrinsic ambiguities in this estimate of an astrophysical nature that may reduce or extend the time required for a 5σ observation [53]. In particular, the poorly known extended nature of some of the Milagro sources and the value of the cutoff represent a challenge for IceCube analyses that are optimized for point sources. The absence of any observation of an accumulation of high energy neutrinos in the direction of these sources will seriously challenge the concept that gamma ray telescopes are seeing actual sources of cosmic rays.

These predictions have been stable over the years and have recently been updated in the context of new gamma ray information, especially from the HAWC experiment; see reference [56].

3.3 Generic Fireballs

Whereas we have confidence that the electromagnetic radiation in some Galactic sources is produced by the decay of neutral pions, there is no straightforward gamma-ray path to the neutrino flux expected from extragalactic cosmic-ray accelerators. We presented model calculations to show that AGNs can plausibly accommodate the cosmic neutrino flux observed, assuming that they accelerate protons at the level of the sources of the extragalactic cosmic rays. In fact, we showed how very different blueprints for the beam dump can fit the diffuse neutrino flux observed. As already discussed, there is an yet another possibility. Massive stars collapsing to black holes and observed by astronomers as GRBs have the potential to accelerate protons to 100 EeV energy. Neutrinos of $100\,\mathrm{TeV} - \mathrm{PeV}$ energy should be produced by pion photoproduction when protons and photons coexist in the GRB fireball [62]. As previously discussed, the model is promising because the observed cosmic-ray flux can be accommodated with the assumption that roughly equal energy is shared by electrons, observed as synchrotron photons, and protons. Indeed, the IceCube observations indicate equal extragalactic energy densities of photons and neutrinos, as we will see further on.

The phenomenology that successfully accommodates the astronomical observations is the creation of a hot fireball of electrons, photons, and protons that is initially opaque to radiation. The hot plasma therefore expands by radiation pressure, and particles are accelerated to a Lorentz factor Γ that grows until the plasma becomes optically thin and produces the GRB display. From this point on, the fireball coasts with a Lorentz factor that is constant and depends on its baryonic load. The baryonic component carries the bulk of the fireball's kinetic energy. The energetics and rapid time structure of the burst can be successfully associated with successive shocks (shells), of width ΔR, that develop in the expanding fireball. The rapid temporal variation of the gamma-ray burst, t_v, is on the order of milliseconds and can be interpreted as the collision of internal shocks with a varying baryonic load leading to differences in the bulk Lorentz factor. Electrons, accelerated by first-order Fermi acceleration, radiate

synchrotron gamma rays in the strong internal magnetic field and thus produce the spikes observed in the burst spectra.

The usual approach followed in the interpretation of routine IceCube GRB searches [63] has the proton content of the fireball derived from the observed electromagnetic emission. The basic assumption is that a comparable amount of energy is dissipated in fireball protons and electrons, where the latter are observed as synchrotron radiation,

$$E^2 \frac{dN_\nu}{dE} = \left(\frac{\epsilon_p}{\epsilon_e}\right) \frac{1}{2}\, x_\nu \left[E_\gamma^2 \frac{dN_\gamma}{dE_\gamma}(E_\gamma)\right]_{\rm syn}, \tag{33}$$

where ϵ_p and ϵ_e are the energy fractions in the fireball in protons and electrons [63], respectively. One can then use the data to determine the baryon loading in the GRB fireball, $\epsilon_p \,/\, \epsilon_e$. No predictions are made. The abundance of protons in the fireball is determined, or, at present, limited by the observations [37].

Although simulations of GRB fireballs have reached a level of sophistication [64], a simple energy estimate is sufficient to predict the neutrino flux associated with GRB fireballs assuming that they are the sources of the cosmic rays.

Simple relativistic kinematics (see Fig. 9) relates the radius and width R' and $\Delta R'$ to the observed duration of the photon burst $c\Delta t$:

$$R' = \gamma^2 (c\Delta t) \tag{34}$$

$$\Delta R' = \gamma c \Delta t \tag{35}$$

From the observed GRB luminosity L_γ, we compute the photon energy density in the shell:

$$U'_\gamma = \frac{(L_\gamma \Delta t)\,/\gamma}{4\pi R'^2 \Delta R'} = \frac{L_\gamma}{4\pi \Delta t^2 c^3 \gamma^6} \tag{36}$$

The pion production by shocked protons in this photon field is, as before, calculated from the interaction length:

$$\frac{1}{\lambda_{p\gamma}} = N_\gamma \sigma_\Delta \langle x_{p\to\pi}\rangle = \frac{U'_\gamma}{E'_\gamma} \sigma_\Delta \langle x_{p\to\pi}\rangle \qquad \left(E'_\gamma = \frac{1}{\gamma} E_\gamma\right). \tag{37}$$

Also as before, σ_Δ is the cross section for $p\gamma \to \Delta \to n\pi^+$ and $\langle x_{p\to\pi}\rangle \simeq 0.2$. The fraction of energy going into π-production is

$$f_\pi \cong \frac{\Delta R'}{\lambda_{p\gamma}} \tag{38}$$

$$f_\pi \simeq \frac{1}{4\pi c^2} \frac{L_\gamma}{E_\gamma} \frac{1}{\gamma^4 \Delta t} \sigma_\Delta \langle x_{p\to\pi}\rangle \tag{39}$$

$$f_\pi \simeq 0.14 \left[\frac{L_\gamma}{10^{51}\,{\rm ergs}^{-1}}\right] \left[\frac{1\ {\rm MeV}}{E_\gamma}\right] \left[\frac{300}{\gamma}\right]^4 \left[\frac{1\ {\rm msec}}{\Delta t}\right] \times \left[\frac{\sigma_\Delta}{10^{-28}\,{\rm cm}^2}\right] \left[\frac{\langle x_{p\to\pi}\rangle}{0.2}\right]. \tag{40}$$

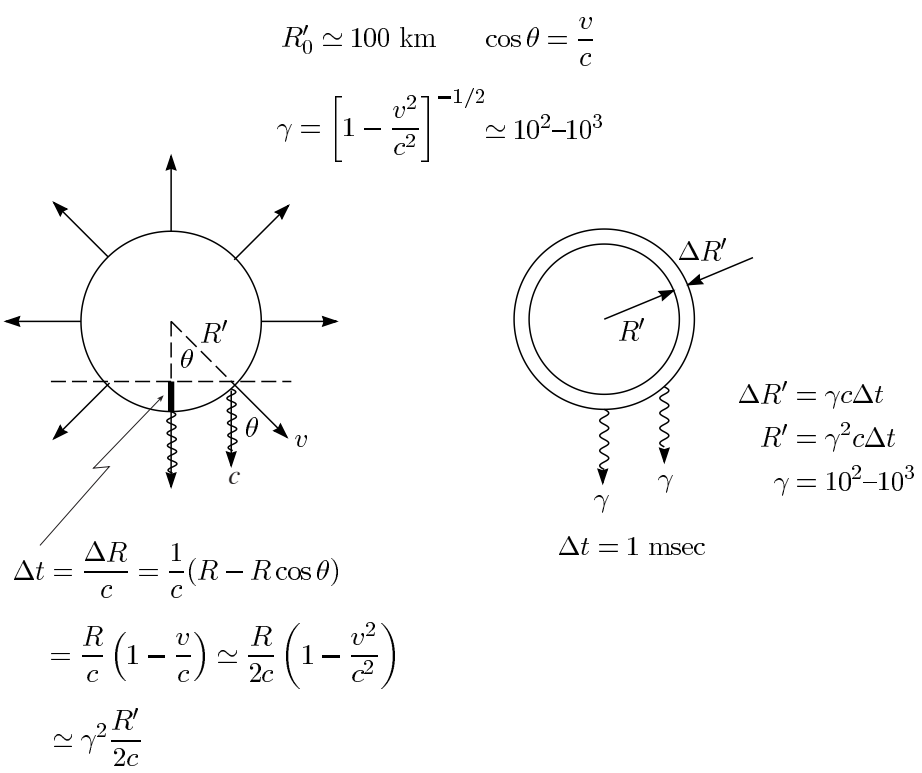

Figure 9: Kinematics of GRB fireballs. Kinematics of a relativistically expanding fireball, and on the right, the resulting shell(s) expanding under radiation pressure.

The relevant photon energy in the problem is 1 MeV, the energy where the typical GRB spectrum exhibits a break. The contribution of higher energy photons is suppressed by the falling spectrum, and lower energy photons are less efficient at producing pions. Given the large uncertainties associated with the astrophysics, it is an adequate approximation to neglect the explicit integration over the GRB photon spectrum. The proton energy for production of pions via the Δ-resonance is

$$E'_p = \frac{m_\Delta^2 - m_p^2}{4E'_\gamma}. \tag{41}$$

Therefore,

$$E_p = 1.4 \times 10^{16}\,\mathrm{eV}\left(\frac{\gamma}{300}\right)^2\left(\frac{1\ \mathrm{MeV}}{\mathrm{E}_\gamma}\right) \tag{42}$$

$$E_\nu = \frac{1}{4}\langle x_{p\to\pi}\rangle\, E_p \simeq 7 \times 10^{14}\,\mathrm{eV}. \tag{43}$$

We are now ready to calculate the neutrino flux:

$$\frac{dN_\nu}{dE_\nu} = \frac{c}{4\pi}\frac{U'_\nu}{E'_\nu} = \frac{c}{4\pi}\frac{U_\nu}{E_\nu} = \frac{c}{4\pi}\frac{1}{E_\nu}\left[\frac{1}{2}f_\pi t_H \dot{E}\right], \tag{44}$$

where the factor 1/2 accounts for the fact that only 1/2 of the energy in charged pions is transferred to $\nu_\mu + \bar{\nu}_\mu$. As before, $\dot{E}$ is the injection rate in cosmic rays beyond the ankle ($\sim 4 \times 10^{44}\,\mathrm{erg\,Mpc^{-3}\,yr^{-1}}$) and t_H is the Hubble time of $\sim 10^{10}$ Gyr. Numerically,

$$\begin{aligned}\frac{dN_\nu}{dE_\nu} &= 2\times 10^{-14}\,\mathrm{cm^{-2}\,s^{-1}\,sr^{-1}}\left[\frac{7\times 10^{14}\,\mathrm{eV}}{\mathrm{E}_\nu}\right]\left[\frac{f_\pi}{0.125}\right]\left[\frac{t_H}{10\ \mathrm{Gyr}}\right] \\ &\quad\times\left[\frac{\dot{E}}{10^{44}\,\mathrm{erg\,Mpc^{-3}\,yr^{-1}}}\right]\end{aligned} \tag{45}$$

The only subtlety here is the γ^2 dependence of the shell radius R'; for a simple derivation, see Ref. [6]. The result is insensitive to beaming. Beaming yields more energy per burst, but fewer bursts are actually observed. The predicted rate is also insensitive to the neutrino energy E_ν because higher average energy yields fewer νs, but more are detected. Both effects are approximately linear. Neutrino telescopes are essentially background free for such high-energy events and should be able to identify neutrinos at all zenith angles.

For typical choices of the parameters, $\gamma \sim 300$ and $t_v \sim 10^{-2}s$, about 100 events per year are predicted in IceCube, a flux that was already challenged [65] by the limit on a diffuse flux of cosmic neutrinos obtained with one-half of IceCube in one year [66]. As before, the energy density of extragalactic cosmic rays of $\sim 10^{44}$ TeV $\mathrm{Mpc^{-3}\ yr^{-1}}$ depends on the unknown transition energy between the Galactic and extragalactic components of the spectrum. In the end, the predictions can be stretched, but having failed by now to observe high-energy neutrinos in spacial and temporal coincidence with over 1000 GRB observations, IceCube has set a limit that is less than 1% of the PeV cosmic neutrino flux actually observed.

We have nevertheless discussed fireballs in some detail to illustrate their potential as cosmic accelerators and to point out that they may produce cosmic neutrinos without being the sources of cosmic rays. For instance, they may produce neutrinos of lower energy in events where the boost factor is limited, $\gamma \leq 10$. Candidate events have been observed and are referred to as "low luminosity GRBs." [67] There is also the possibility that high-energy gamma rays and neutrinos are produced when the shock expands further into the interstellar medium. This mechanism has been invoked as the origin of the delayed high-energy gamma rays. Adapting the previous calculation to the external shock is straightforward. For instance, following Bottcher et al. [68], we find that the time scale is changed from milliseconds to seconds and the break in the spectrum from 1 to 0.1 MeV, and that f_π is reduced by two orders of magnitude. In the external shocks, higher energies can be reached, possibly a factor of 10 higher than for Bottcher et al. model). This increases the neutrino detection

efficiency. In the end, the observed rates are an order of magnitude smaller, but the inherent ambiguities of the estimates are such that it is difficult to establish with confidence the relative rate in internal and external shocks.

3.4 Dedicated Search for EeV-Energy Neutrinos from GZK Interactions

Whatever the sources of the extragalactic cosmic rays may be, a cosmogenic flux of neutrinos, often dubbed GZK flux, originates from the interactions of cosmic rays with the cosmic microwave background (CMB). Produced by a source located at a cosmological distance, a GZK neutrino will point back to it with subdegree precision. The calculation of the GZK neutrino flux is relatively straightforward, and its magnitude is predominantly determined by the total energy density of cosmic rays in the universe; as before, the crossover from the Galactic to the extragalactic component is a critical parameter. A sample calculation [69] is shown in Fig. 10. It is also important to realize that, among the $p\,\gamma$ final-state products produced via the decay of pions, GZK neutrinos are accompanied by a flux of electrons, positrons, and gamma rays that quickly cascades to lower energies in the CMB and intergalactic magnetic fields. An electromagnetic cascade develops with a maximum in the GeV-TeV energy region. Here, the total energy in the electromagnetic cascade is constrained by Fermi-LAT measurements of the diffuse extragalactic gamma-ray background [70].

For the flux shown in Fig. 10, we anticipate 2.3 events in three years of running the completed IceCube detector, assuming the best fit from the figure, and 4.8 events for the highest flux consistent with the Fermi constraint. These have not yet been seen [71]; see Fig. 11. Note however that the anticipated event rate has been obtained assuming that the highest energy cosmic rays are protons. Experiments disagree on the composition of particles around $10^{20}\,\mathrm{eV}$ [72]. While the cosmic-ray energy density and the other parameters in the calculation (cosmological evolution, energy dependence of the injected cosmic-ray flux, and its maximum energy) can still be manipulated to explain the failure by IceCube to observe GZK neutrinos, the result may hint at a heavy composition for the highest energy particles. Hopefully, the ongoing upgrades of the TA and Auger experiments will resolve this issue.

4 Instrumentation: The First Kilometer-Scale Neutrino Detector

As previously discussed, the rationale for kilometer-scale neutrino detectors is that their sensitivity is sufficient to reveal generic cosmic-ray sources with an energy density in neutrinos comparable to their energy density in cosmic and pionic TeV gamma rays. By the turn of the century, a series of first-generation experiments [77, 78] demonstrated that high-energy neutrinos with $\sim 10\,\mathrm{GeV}$ energy and above could be detected by observing Cherenkov radiation from

secondary particles produced in neutrino interactions inside large volumes of highly transparent ice or water instrumented with a lattice of photomultiplier tubes. Construction of the first second-generation detector, IceCube, at the geographic South Pole was completed in December 2010 [79]; see Fig. 12.

4.1 IceCube

IceCube consists of 80 strings, each instrumented with 60 10-inch photomultipliers spaced by 17 m over a total length of 1 kilometer. The deepest module is located at a depth of 2.450 km so that the instrument is shielded from the large background of cosmic rays at the surface by approximately 1.5 km of ice. Strings are arranged at apexes of equilateral triangles that are 125 m on a side. The instrumented detector volume is a cubic kilometer of dark, highly transparent and sterile Antarctic ice. Radioactive background is dominated by the instrumentation deployed into this natural ice.

Each optical sensor consists of a glass sphere containing the photomultiplier and the electronics board that digitizes the signals locally using an on-board computer. The digitized signals are given a global time stamp with residuals accurate to less than 3 ns and are subsequently transmitted to the surface. Processors at the surface continuously collect these time-stamped signals from the optical modules, each of which functions independently. The digital messages are sent to a string processor and a global event trigger. They are subsequently sorted into the Cherenkov patterns emitted by secondary muon tracks, or electron and tau showers, that reveal the direction of the parent neutrino [80].

As will be discussed further on, similar detectors are planned for deployment in deep transparent Mediterranean water [81] and in Lake Baikal.

4.2 Detection Methods

Neutrino telescopes exploit the relatively large neutrino cross section and the long muon range above TeV energies to achieve a detection efficiency sufficient to reach the predicted point source and diffuse fluxes previously discussed. At the same time, detecting ν_e and ν_τ neutrinos cannot be ignored; the case has been made in detail in Ref. [13]. The detection of neutrinos of all flavors is important in separating diffuse extraterrestrial neutrinos from atmospheric neutrinos. Generic cosmic accelerators produce neutrinos from the decay of pions with admixture $\nu_e : \nu_\mu : \nu_\tau = 1 : 2 : 0$. Over cosmic baselines, neutrino oscillations transform the ratio to $1 : 1 : 1$, because approximately one-half of the ν_μ convert to ν_τ.

IceCube detects neutrinos by observing the Cherenkov radiation from the charged particles produced by neutrino interactions inside or in the vicinity of the detector. Charge current interactions produce a lepton that carries, on average, 50% of the neutrino energy for $E \leq 10\,\mathrm{GeV}$, to 80% at high energies; the remainder of the energy is released in the hadronic shower produced by the target nucleus. Both the secondary lepton and the hadronic shower produce Cherenkov radiation. In neutral current interactions, the neutrino transfers a

fraction of its energy to a nuclear target, producing a hadronic shower. IceCube can differentiate neutrino flavors on the basis of their topology in the detector, as illustrated in Fig. 13. There are two basic topologies: tracks from ν_μ and cascades from ν_e, ν_τ, and the neutral current interactions from all flavors. On the scale of IceCube, PeV cascades have a length of less than 10 m and are therefore point sources of Cherenkov light in a detector of kilometer size.

Neutrino telescopes also measure neutrino energy. Muons range out, over kilometers at TeV energy to tens of kilometers at EeV energy, generating showers along their track by bremsstrahlung, pair production, and photonuclear interactions. The charged particles produced are the sources of additional Cherenkov radiation. Because the energy of the muon degrades along its track, the energy of the secondary showers decreases, which reduces the distance from the track over which the associated Cherenkov light can trigger a PMT. The geometry of the light pool surrounding the muon track is therefore a kilometer-long cone with a gradually decreasing radius. In its first kilometer, a high-energy muon typically loses energy in a couple of showers having one-tenth of the muon's initial energy. So the initial radius of the cone is the radius of a shower with 10% of the muon energy. At lower energies of hundreds of GeV and less, the muon becomes minimum-ionizing.

Because of the stochastic nature of the muon's energy loss, the relationship between the observed energy loss inside the detector and muon energy varies from muon to muon. Additionally, only the muon energy lost in the detector can be determined; we do not know its energy loss before entering the instrumented volume nor how much energy it carries out upon exiting. An unfolding process is required to determine the neutrino energy based on the observed muon energy; fortunately, it is based on well-understood Standard Model physics. In contrast, for ν_e and ν_τ, the detector is a total energy calorimeter, and the determination of their energy is superior.

The different topologies each have advantages and disadvantages. For ν_μ interactions, the long lever arm of muon tracks, up to tens of kilometers at very high energies, allows the muon direction (and the neutrino direction) to be determined accurately with an angular resolution measured online that is better than 0.4°. Superior angular resolution can be reached for selected events. Sensitivity to point sources is therefore better as well. The disadvantages are a large background, of atmospheric neutrinos below 100 TeV and cosmic-ray muons at all energies, and the indirect determination of the neutrino energy that must be inferred from sampling the energy loss of the muon when it transits the detector.

Observation of ν_e and ν_τ flavors represents significant advantages. They are detected for both Northern and Southern Hemispheres. (This is also true for ν_μ with energy in excess of 1 PeV, where the background from the steeply falling atmospheric spectrum becomes negligible.) At TeV energies and above, the background of atmospheric ν_e is lower by over an order of magnitude, and there are essentially no atmospheric ν_τ produced. At higher energies, long-lived pions, the source of atmospheric ν_e, no longer decay, and relatively rare K-decays become the dominant source of background ν_e. Furthermore, because the neutrino

events are totally, or at least partially, contained inside the instrumented detector volume, the neutrino energy is determined by total-absorption calorimetry. One can establish the cosmic origin of a single event by demonstrating that the energy cannot be reached by muons and neutrinos of atmospheric origin. Finally, ν_τ are not absorbed by the Earth [82]: ν_τ interacting in the Earth produce secondary ν_τ of lower energy, either directly in a neutral current interaction or via the decay of a secondary tau lepton produced in a charged-current interaction. High-energy ν_τ will thus cascade down to energies of hundred of TeV where the Earth becomes transparent. In other words, they are detected with a reduced energy but not absorbed.

Although cascades are nearly pointlike and, in practice, spatially isotropic, the pattern of arrival times of the photons at individual optical modules reveals the direction of the secondary leptons with 3°. While a fraction of cascade events can be reconstructed accurately to within a degree [83], the precision is inferior to that reached for ν_μ events and typically not better than 10° using the present techniques.

At energies above about 100 PeV, electromagnetic showers begin to elongate because of the Landau-Pomeranchuk-Migdal effect [84]. An extended length scale is associated with the abundant radiation of soft photons that results in interactions of the shower particles on two target atoms. Negative interference in this process results in reduced energy loss.

4.3 Detector Performance

Cosmic neutrinos must be separated from the large backgrounds of atmospheric neutrinos and atmospheric cosmic-ray muons. This is possible for two classes of events: neutrinos that interact inside the instrumented volume ("starting events") and events where a muon enters the detector from below, created by a neutrino traversing the Earth (throughgoing events), thus pointing back to its origin. In this latter case, the Earth is used as a filter for cosmic-ray muons.

For starting events, the pathlength $l(\theta)$ traversed within the detector volume by a neutrino with zenith angle θ is determined by the detector's geometry. Neutrinos are detected if they interact within the detector volume, i.e., within the instrumented volume of one cubic kilometer. That probability is

$$P(E_\nu) = 1 - \exp[-l/\lambda_\nu(E_\nu)] \simeq l/\lambda_\nu(E_\nu)\,, \tag{46}$$

where $\lambda_\nu(E_\nu) = [\rho_{\rm ice}\ N_A\ \sigma_{\nu N}(E_\nu)]^{-1}$ is the mean free path in ice for a neutrino of energy E_ν. Here, $\rho_{\rm ice} = 0.9$ g cm^{-3} is the density of the ice, $N_A = 6.022 \times 10^{23}$ is Avogadro's number, and $\sigma_{\nu N}(E_\nu)$ is the neutrino-nucleon cross section. A neutrino flux dN/dE_ν (neutrinos per GeV per cm^2 per second) crossing a detector with energy threshold and cross sectional area $\mathrm{A}(E_\nu)$ facing the incident beam will produce

$$N_{ev} = T \int_{E_\nu^{\rm th}} A(E_\nu)\, P(E_\nu)\, \frac{dN}{dE_\nu}\, dE_\nu \tag{47}$$

events after a time T. The "effective" detector area $\mathrm{A}(E_\nu)$ is also a function of the zenith angle θ. It isn't strictly equal to the geometric cross section of the instrumented volume facing the incoming neutrino, because even neutrinos interacting outside the instrumented volume may produce enough light inside the detector to be detected. In practice, $\mathrm{A}(E_\nu)$ is determined as a function of the incident neutrino direction and zenith angle by a full-detector simulation, including the trigger.

This formalism applies to contained events. For muon neutrinos, any neutrino producing a secondary muon that reaches the detector (and has sufficient energy to trigger it) will be detected. Because the muon travels kilometers at TeV energy and tens of kilometers at PeV energy, neutrinos can be detected outside the instrumented volume; the probability is obtained by substitution in Eq. 46,

$$l \to \lambda_\mu \,, \tag{48}$$

thereby giving,

$$P = \lambda_\mu / \lambda_\nu \,. \tag{49}$$

Here, λ_μ is the range of the muon determined by its energy losses. Values for the neutrino nucleon cross section and the range of the muon can be found in Ref. [20]

The complete expression for the flux of ν_μ-induced muons at the detector is given by a convolution of the neutrino spectrum ϕ $(= dN/dE_\nu)$ with the probability P to produce a muon reaching the detector [4, 5, 6]:

$$\phi_\mu(E_\mu^{\min}, \theta) = \int_{E_\mu^{\min}} P(E_\nu, E_\mu^{\min}) \, \exp[-\sigma_{\mathrm{tot}}(E_\nu) \, N_A \, X(\theta)] \, \phi(E_\nu, \theta) dE_\nu. \tag{50}$$

The additional exponential factor accounts for the absorption of neutrinos along a chord of the Earth of length $X(\theta)$ at zenith angle θ. Absorption becomes important for $\sigma_\nu(E_\nu) \gtrsim 10^{-33}\,\mathrm{cm}^2$ or $E_\nu \gtrsim 100$ TeV. For back-of-the-envelope calculations, the P-function can be approximated by

$$P \simeq 1.3 \times 10^{-6} E^{2.2} \qquad \text{for } E = 10^{-3}\text{–}1 \text{ TeV} \,, \tag{51}$$

$$\simeq 1.3 \times 10^{-6} E^{0.8} \qquad \text{for } E = 1\text{–}10^3 \text{ TeV} \,. \tag{52}$$

At EeV energy, the increase is reduced to only $E^{0.4}$. Clearly, high-energy neutrinos are more likely to be detected because of the increase with energy of both the cross section and muon range.

Tau neutrinos interacting outside the detector can be observed provided the tau lepton they produce reaches the instrumented volume within its lifetime. In Eq. 46, l is replaced by

$$l \to \gamma c\tau = E/mc\tau \,, \tag{53}$$

where m, τ, and E are the mass, lifetime, and energy of the tau, respectively. The tau's decay length $\lambda_\tau = \gamma c\tau \approx 50 \text{ m} \times (E_\tau/10^6)$ GeV grows linearly with energy and actually exceeds the range of the muon near 1 EeV. At yet higher energies, the tau eventually ranges out by catastrophic interactions, just like

the muon, despite the reduction of the energy-loss cross sections by a factor of $(m_\mu/m_\tau)^2$.

Tracks and showers produced by tau neutrinos are difficult to distinguish from those initiated by muon and electron neutrinos, respectively. To be clearly identified, both the initial neutrino interaction and the subsequent tau decay must be contained within the detector; for a cubic- kilometer detector, this happens for neutrinos with energies from a few PeV to a few tens of PeV [85].

For an in-depth discussion of neutrino detection, energy measurement, and flavor separation, and for detailed references, see the IceCube Preliminary Design Document [13] and Ref. [2].

4.4 Atmospheric Neutrinos

Muons and neutrinos from decay of mesons produced by cosmic-ray interactions in the atmosphere are the background in the search for neutrinos of extraterrestrial origin. The 3 kHz trigger rate of IceCube is dominated by atmospheric muons from decay of pions and kaons produced in the atmosphere above the detector. The distribution peaks near the zenith and decreases with increasing angle as the muon energy required to reach the deep detector increases. Most atmospheric muons are easily identified as entering tracks from above and rejected. Because of the large ratio of muons to neutrinos, however, misreconstructed atmospheric muons remain an important source of background for all searches.

Measurement of the spectrum of atmospheric neutrinos is an important benchmark for a neutrino telescope. IceCube detects an atmospheric neutrino every six minutes. The spectrum of atmospheric ν_μ has been measured by unfolding the measured rate and energy deposition of neutrino-induced muons entering the detector from below the horizon [31], as shown in Fig. 6. More challenging is the measurement of the flux of atmospheric electron neutrinos. This has been done by making use of DeepCore, the more densely instrumented subarray in the deep center of IceCube, to identify contained shower events. The known spectrum of ν_μ is used to calculate the contribution of neutral current interactions to the observed rate of showers. Subtracting the neutral current contribution leads to the measurement of the spectrum of atmospheric electron neutrinos from 100 GeV to 10 TeV [33], as shown in Fig. 6.

In general, atmospheric neutrinos are indistinguishable from astrophysical neutrinos. An important exception occurs in the case of muon neutrinos from above when the neutrino energy is sufficiently high and the zenith angle sufficiently small that the muon produced in the same decay as the neutrino is guaranteed to reach the detector [86]. This is used to reject atmospheric neutrinos in analyses where they are a background. Monte Carlo simulation can be used to evaluate the atmospheric neutrino passing rate more generally by also including other high-energy muons produced in the same cosmic-ray shower as the neutrino. In this way, the method can be extended to electron neutrinos. In practice, the passing rate is significantly reduced for zenith angles $\theta < 70^\circ$ and $E_\nu > 100$ TeV.

The spectrum of atmospheric neutrinos becomes one power steeper than the spectrum of primary nucleons at high energy as the competition between interaction and decay of pions and kaons increasingly suppresses their decay. For the dominant kaon channel, the characteristic energy for the steepening is $E_\nu \sim 1 \text{ TeV}/\cos\theta$. A further steepening occurs above 100 TeV as a consequence of the knee in the primary spectrum. Astrophysical neutrinos should reflect the cosmic-ray spectrum in the source and are therefore expected to have a significantly harder spectrum than atmospheric neutrinos. Establishing an astrophysical signal above the steep atmospheric background requires an understanding of the atmospheric neutrino spectrum around 100 TeV and above.

Although there is some uncertainty associated with the composition through the knee region [87], the major uncertainty in the spectrum of atmospheric neutrinos at high energy is the level of charm production. The short lived charmed hadrons preferentially decay up to a characteristic energy of 10^7 GeV, producing prompt muons and neutrinos with the same spectrum as their parent cosmic rays. This prompt flux of leptons has not yet been measured. Existing limits [88, 89] allow a factor of two or three around the level predicted by a standard calculation [36] (after correction for steepening at the knee). For reasonable assumptions, the charm contribution is expected to dominate the conventional spectrum above ~ 10 TeV for ν_e, above ~ 100 TeV for ν_μ, and above ~ 1 PeV for muons [90].

The expected hardening in the spectrum of atmospheric neutrinos due to prompt neutrinos is partially degenerate with a hard astrophysical component. However, the spectrum of astrophysical neutrinos should reflect the spectrum of cosmic rays at their sources, which is expected to be harder than the spectrum of cosmic rays at Earth. It should eventually be possible with IceCube to measure the charm contribution by requiring a consistent interpretation of neutrino flavors and cosmic-ray muons for which there is no astrophysical component. An additional signature of atmospheric charm is the absence of seasonal variations for this component [91].

5 Cosmic Neutrinos

There are two primary methods used to identify neutrinos. As previously discussed, neutrino searches have historically focused on the observation of muon neutrinos that interact primarily outside the detector, producing kilometer-long muon tracks that pass through the detection volume. Although this allows observation of neutrinos that interact outside the detector, it is then necessary to use the Earth as a filter in order to remove the huge background of cosmic-ray muons. Even at a depth of 1,450 meters, IceCube detects atmospheric cosmic-ray muons originating in the Southern Hemisphere at a rate of 3,000 per second. This method limits the neutrino view to a single flavor and half the sky. An alternative method exclusively identifies neutrinos interacting inside the detector. It divides the instrumented volume of ice into an outer veto shield and

a roughly 500 megaton inner fiducial volume. The advantage of focusing on neutrinos interacting inside the instrumented volume of ice is that the detector then functions as a total absorption calorimeter, measuring energy with a 10-15 % resolution. Also, neutrinos from all directions in the sky can be identified, including both muon tracks, produced in muon-neutrino charged-current interactions, and secondary showers, produced by electron and tau neutrinos as well as in neutral-current interactions of neutrinos of all flavors. The Cherenkov patterns initiated by an electron (or tau) neutrino of 1 PeV, or petaelectronvolt (10^{15} eV), energy and by a muon neutrino depositing 2.6 PeV energy while traversing the detector are contrasted in Fig. 14.

In general, the particle's trajectory is determined from the arrival times of photons at the optical sensors [92], while the number of photons is a proxy for the amount of energy deposited. The two methods for separating neutrinos from the cosmic-ray muon background have complementary advantages. The long tracks produced by muon neutrinos can point back to their sources with a 0.4° angular resolution. In contrast, the reconstruction of the direction of secondary showers, still in the development stage in IceCube [93], can be determined to within $10^\circ \sim 15^\circ$ of the direction of the incident neutrino. Determining the deposited energy from the observed light pool is, however, relatively straightforward, and a resolution of better than 15% is possible.

For neutrino astronomy, the first challenge is to select sufficiently pure samples of neutrinos: roughly 100,000 per year in a background of ten billion cosmic-ray muons. The second is to identify the small fraction of the sample that are neutrinos of astrophysical origin, expected at the level of tens of events per year. Atmospheric neutrinos are an overwhelming background for cosmic neutrinos, at least at energies below $\sim$ 100 TeV. Above this energy, however, the atmospheric neutrino flux is too small to produce events even in a kilometer-scale detector, and every event observed in that range represents the discovery of an astrophysical neutrino.

By now, IceCube has observed cosmic neutrinos using both methods for rejecting background, and each analysis has reached a statistical significance of more than 5σ [94, 95]. Based on different methods for reconstruction and energy measurement, the results agree, pointing at extragalactic sources whose flux has equilibrated in the three flavors after propagation over cosmic distances. Its total energy matches that of extragalactic photons and cosmic rays.

5.1 Evidence for Cosmic Neutrinos

IceCube is sensitive to neutrinos with energies above a threshold of approximately 0.1 TeV. Using the Earth as a filter, a flux of neutrinos has been identified that is consistent with atmospheric origin; see Fig. 15. However, in seven years of data, an excess of events has been observed with 5.6σ significance at energies beyond 100 TeV [96, 97, 95] that cannot be accommodated by the atmospheric flux. Whereas IceCube only measures the energy deposited by the secondary muon inside the detector, Standard Model physics allows one to infer the energy spectrum of the parent neutrinos, as illustrated in Fig. 15. For the

highest energy event, shown in Fig. 14, the most likely energy of the parent neutrino is almost 10 PeV. The muon energy loss measured in the detector is 2.6 ± 0.3 PeV. The cosmic flux is well described by a power law with a spectral index of 2.13 ± 0.13 and a normalization at 100 TeV neutrino energy of $(0.9 \pm 0.3) \times 10^{-18}\,\mathrm{GeV}^{-1}\mathrm{cm}^{-2}\mathrm{sr}^{-1}$. The neutrino energy contributing to this flux covers the range of 200 TeV to 9 PeV. As will be discussed further on, we will find that analyses that extend to lower energies reveal an excess of neutrino events over the atmospheric background in the $30 \sim 100$ TeV energy range, well above the extrapolation of the cosmic muon neutrino flux to lower energies. The conclusion to be drawn is that the astrophysical flux measured by IceCube is not featureless.

The first hint of cosmic neutrinos emerged when two events were found serendipitously in a search for GZK neutrinos using IceCube data collected between May 2010 and May 2012 [98]. The energies of these neutrinos, rather than EeV as expected for GZK neutrinos, were in the PeV range: 1.040 PeV and 1.140 PeV. The events were particle showers initiated by electron or tau neutrinos interacting inside the instrumented detector volume. Their light pool of roughly one hundred thousand photoelectrons extended over more than 500 meters; one of them is shown in Fig. 14. With PeV energy and no trace of accompanying muons from an atmospheric shower, they are unlikely to be atmospheric in origin. It is indeed important to realize that the muon produced in the same pion or kaon decay as an atmospheric neutrino is guaranteed to reach the detector provided that the neutrino energy is sufficiently high and the zenith angle sufficiently small [86, 99]. In this case, the atmospheric neutrino provides its own self-veto. This self-veto is routinely applied to IceCube cosmic neutrino candidates that consist exclusively of isolated neutrino events.

The observation of these two neutrinos immediately suggested an analysis that searched for neutrinos originating inside the detector, their well-measured energy allowing a clear separation between neutrinos of atmospheric origin and those of cosmic origin. The geometry of the veto and active signal regions was optimized to reduce the background of atmospheric muons and neutrinos to a handful of events per year while keeping 98% of the cosmic signal. In analyzing the data covering the same time period as the GZK neutrino search, 28 candidate neutrino events were identified with in-detector deposited energies between 30 and 1140 TeV. Of these, 21 were showers. The remaining seven events were muon tracks. The 28 events include the two PeV events previously revealed in the GZK neutrino search.

The energy and zenith angle dependence observed is consistent with expectations for a flux of neutrinos produced by cosmic accelerators; see Fig. 16. The flavor composition of the flux is, after corrections for the acceptances of the detector to the different flavors, consistent with $\nu_e : \nu_\mu : \nu_\tau \sim 1 : 1 : 1$, as anticipated for a flux originating in cosmic sources. It is also consistent with the flux of muon neutrinos penetrating the Earth, as shown in Fig. 15. Subsequently, two additional years of data have been analyzed, doubling the statistics of the published discovery results [101]. A purely atmospheric explanation can be excluded at 7σ. The four-year data set contains a total of 54 neutrino events with

deposited energies ranging from 30 to 2000 TeV. In the fourth year, muon tracks were found that deposited $\sim 500\,\mathrm{TeV}$ energy inside the detector, produced by PeV-energy parent neutrinos. One of them reconstructs through IceTop, IceCube's surface array, with no evidence for an air shower. Combining the absence of an air shower in IceTop with large deposited muon energy results in a high significance for astrophysical origin from a single event.

In summary, both methods for selecting cosmic neutrinos harvest about 10 to 15 events per year, more if one tolerates a modest background. With six years of data from the completed detector, our data sample exceeds one hundred events, approaching the statistics required to identify their origins by matching arrival directions with astronomical maps [102].

5.2 Origin of Cosmic Neutrinos

Figure 17 shows in Galactic coordinates the arrival directions of cosmic neutrinos for four years of events with interaction vertices inside the detector. Shower events are labeled (+), track events (×). The color scale indicates the value of the test statistic of an unbinned maximum likelihood test searching for anisotropies of the neutrino arrival directions. This measured distribution corresponds to no significant local excess in the sky; the probability of obtaining the measured anisotropy in randomized pseudo-experiments is 58%. The correlation of neutrino events with the Galactic plane is not significant. Letting the width of the plane float freely, the best fit returned a correlation for a value of $\pm 7.5^\circ$ with a posttrial chance probability of 3.3%. Neither probability increased after doubling the data from two to four years.

In short, the observed neutrino flux is consistent with an isotropic distribution of arrival directions and equal contributions of all neutrino flavors [103]. A subdominant Galactic component of the flux cannot be excluded at this time. Interestingly, a variety of analyses [103, 104] suggest that the cosmic neutrino flux dominates the atmospheric background above an energy that may be as low as 30 TeV, with an energy spectrum that cannot described as a single power as was the case for the muon neutrino flux through the Earth for energies exceeding 220 TeV. This observation is reinforced by the fact that fitting the cosmic neutrino flux in different ranges of energy yields values for the power-law exponent that are statistically inconsistent.

Rather than speculate on their origin, we will focus on the multimessenger connection of cosmic neutrinos to cosmic rays and gamma rays; this will turn out to be revealing. Neutrinos are produced in association with the cosmic-ray beam. It is straightforward to apply the multimessenger relation derived in section II to the cosmic neutrino flux observed by IceCube. Figure 18 shows the gamma-ray flux accompanying the observed neutrino flux for two illustrative descriptions of the data that assume $K_\pi = 2$. The black and red lines show the neutrino and gamma-ray spectra after accounting for the cascading of the PeV photons in cosmic radiation backgrounds between source and observation. The black line shows an $E^{-2.15}$ neutrino spectrum with an exponential cutoff around PeV. This scenario actually matches the extragalactic isotropic diffuse

gamma-ray background measured by Fermi [105].

The exercise indicates that the contribution of gamma rays accompanying IceCube neutrinos to Fermi's extragalactic flux is significant, suggesting a common origin of some of the sources at some level. This is intriguing because a recent analysis indicates that blazars, active galaxies with the jet pointing at the observer, dominate the Fermi diffuse flux [102]. Are blazars the final answer? The good news is that IceCube, by accumulating more events, can eventually identify blazars by observing multiple neutrinos from the same sources [102]. On the other hand, a search for neutrinos from Fermi's *identified* blazars [107] has come up empty. However, these represent only 50% of the total diffuse background, allowing for the possibility that a partially different source population produces the neutrinos. This could be radio galaxies with misaligned jets, as discussed earlier. Although no definite identification of the sources of cosmic neutrinos has yet emerged, it is rather clear that a multiwavelength path to the neutrino sources looks very promising. Not unexpectedly, evidence for an association has already been claimed by some studies [108, 109, 110, 111].

It is equally remarkable that IceCube's measured energy density in cosmic neutrinos also matches the total energy observed in extragalactic cosmic rays. This is especially interesting because the parents of PeV neutrinos should have energies in the range of 10^{17} eV, well below the ankle in the spectrum at 4×10^{18} eV where traditionally the onset of the extragalactic flux has been theorized.

6 Beyond Astronomy

IceCube was designed as a discovery instrument that covers a range of areas in multidisciplinary science. Examples include the search for Galactic supernova explosions and the study of neutrinos themselves. With higher energies and high-statistics data samples, opportunities for neutrino physics are varied. Also, neutrino telescopes have been recognized as powerful tools in the search for the particle nature of dark matter.

6.1 Searching for Dark Matter

Neutrino telescopes are powerful tools in the search for the particle nature of dark matter. By using the deepest ice and a higher density of optical sensors, IceCube's DeepCore subarray lowers the threshold of the detector to ~ 10 GeV over a significant fraction of the detector volume; see Fig. 12. It was initially proposed as a way to enhance IceCube's capabilities for detecting lower mass dark matter particles. It is worth noting that the AMANDA detector, the forerunner and proof of concept for IceCube, received a significant fraction of its initial funding to search for dark matter. Also, in this context, some have considered the isotropic arrival directions of cosmic neutrinos to be a clue that they originate in the Galactic halo as a result of the decay of PeV-energy dark matter particles, a speculation that at this point is perfectly consistent with

observations [112, 113, 114, 115, 116, 117, 118, 119].

More traditionally, IceCube searches for dark matter by looking for the annihilation of weakly interacting massive particles (WIMPs) wherever they have accumulated to a high density: in the Sun [120], in the Milky Way [121, 122], and in nearby galaxies [123]. For instance, WIMPs are swept up by the Sun as the solar system moves about the Galactic halo. Though interacting weakly, they will occasionally scatter elastically with nuclei in the Sun and lose sufficient momentum to become gravitationally bound. Over the lifetime of the Sun, WIMPs may accumulate to a density where equilibrium is established between their capture and annihilation. The annihilation of these WIMPs to final states that can decay to neutrinos represents an indirect signature of halo dark matter. This WIMP annihilation signal is revealed by the neutrinos that escape the Sun with minimal absorption. The neutrinos are, for instance, the decay products of heavy quarks and weak bosons resulting from the annihilation of WIMPs into $\chi\chi \rightarrow \tau\bar{\tau}$, $b\bar{b}$, or W^+W^-. Neutrino telescopes are sensitive to such neutrinos because of their relatively high energy, above 20 GeV at this point, reflecting the mass of the decaying WIMP.

The beauty of the indirect detection technique using neutrinos originating from the Sun is that the astrophysics of the problem is understood. The source in the Sun has built up over solar time, sampling the dark matter throughout the galaxy. Therefore, any possible structure in the halo has been averaged out. Given a WIMP mass and properties, one can unambiguously predict the signal in a neutrino telescope; if not observed, the model is ruled out. This is in contrast to other indirect searches whose sensitivity depends critically on the structure of halo dark matter; observation requires cuspy structure near the Galactic center or clustering on appropriate scales elsewhere. Observation necessitates not only appropriate WIMP properties but also favorable astrophysical circumstances.

IceCube has established world-leading limits on WIMPs with significant spin-dependent interactions with protons because they result in strong concentrations inside the Sun, a nearby and readily identifiable source [124, 125]. An excess of neutrinos, of GeV or higher energy, over the atmospheric neutrino background in the direction of the Sun is the signature of dark matter. There is no alternative astrophysical explanation of such a signal, which represents a smoking gun for dark matter particles. In most WIMP scenarios, the cross sections for WIMP capture and for WIMP annihilation are large enough so that an equilibrium between capture and annihilation would have been achieved within the age of the solar system [126]. In this case, limits on neutrinos from the Sun can be expressed in terms of the capture cross section. If equilibrium is not reached, weaker limits can still be derived.

The current IceCube limits [120, 124, 125] are shown in Fig. 19. These are derived from three years of muon neutrino observations; no excess of neutrinos over the atmospheric flux has been found in the direction of the Sun. By including events that start inside DeepCore, the mass range for the WIMP search could be extended down to 20 GeV, which overlaps some of the allowed region from the DAMA experiment [127]. Since the exact branching ratios of WIMP annihilation into different channels is model-dependent, experiments usually

choose two annihilation channels that give extreme neutrino spectra to show their results. Annihilation into $b\bar{b}$ is chosen as a representative case producing a soft neutrino spectrum, and annihilation into W^+W^- or $\tau\bar{\tau}$ as a hard spectrum. Assuming a 100% branching ratio to each of these channels brackets the expected neutrino spectrum for any model with branching to more channels. IceCube and Super-K reach bounds at the $10^{-40} - 10^{-41}\text{cm}^2$ level, covering the WIMP mass range, between the two experiments, from a few GeV to 100 TeV. Because of the A^2 coherence factor for scattering on heavy nuclei with atomic number A, the direct detection experiments have an advantage over IceCube for the case of spin-independent interactions. They thus achieve superior limits to IceCube.

6.2 Neutrino Oscillations

The first IceCube neutrino oscillation analysis [134] used data from the 79-string detector from May 2010 to May 2011. The analysis was based entirely on ν_μ-induced muons from below the horizon. By taking advantage of the DeepCore subarray of IceCube, neutrino oscillations were observed over an energy range that includes the oscillation minimum of around 25 GeV for propagation through the diameter of the Earth. Data were divided into two samples, muon tracks reconstructed using the entire IceCube detector ($E_\nu > 100$ GeV) and events starting in DeepCore ($20 < E_\nu < 100$ GeV). The low-energy sample consisted of 719 events, while the high-energy sample included 39,638 events. The high-energy sample, in which standard oscillations do not affect the rates, was used for calibration. A deficit was observed in the low-energy sample, where approximately 25% more events would have been detected in the absence of oscillations. Taking systematic uncertainties into account, including ± 0.05 in the spectral index of the atmospheric neutrino flux at production, the no-oscillation hypothesis was rejected at more than 5σ. The fitted values of the oscillation parameters in a two-flavor fit are $|\Delta m^2_{32}| = 2.3^{+0.5}_{-0.6} \times 10^{-3}$ eV^2 and $\sin^2 2\theta_{23} > 0.93$. For comparison, a recent global three-flavor analysis [135] gives 2.4 eV^2 and 0.95 respectively, with a range of $\pm 5\%$ at 1σ and a slight dependence on the mass hierarchy. While the measured oscillation parameters agree with previous experiments, it is important to realize that they have been measured at a characteristic energy that is higher. The measurement is therefore also sensitive to any new neutrino physics, an important consideration when the precision of the IceCube measurements will be significantly improved.

6.3 Supernovae and Solar Flares

In addition to the normal acquisition of events that reconstruct as tracks or cascades in the deep array of IceCube and as air showers in IceTop, the rates at which the PMT voltages cross the thresholds of discriminators in the DOMs are continuously monitored. Typical rates for DOMs in the deep ice are 500 Hz (including correlated afterpulses), most of which is noise. Typical rates in the

high-gain DOMs of IceTop are 2-5 kHz, most of which is induced by low-energy photons, electrons and muons entering the tanks.

A sudden increase in the total summed counting rate of the deep DOMs would signify a potential supernova explosion in the Galaxy. Supernova neutrinos of ~ 10 MeV interacting within a few meters of a DOM would generate enough hits to cause a sharp increase in the summed counting rate followed by a characteristic decline [136]. IceCube records a DC current that tracks the time evolution of the supernova in microsecond time bins. However, the detector records the time of every photoelectron with nanosecond precision and the binning can therefore be improved offline. This will improve the capability to identify the deleptonization burst. The additional measurement of the rate of neutrino events producing two photons is sensitive to the energy of the supernova neutrinos.

In IceTop, sudden changes in rates occur in response to solar events. Forbush decreases, in which the plasma from a solar flare abruptly reduces the rate of cosmic rays entering the atmosphere, are frequently detected and can be analyzed. More rare are sudden increases caused by solar energetic particles that enter the atmosphere with sufficient energy to generate secondary cosmic rays that reach the IceTop tanks. The event of December 13, 2006, was measured with the sixteen tanks (eight stations) then in operation [137]. The flare of May 17, 2012, is currently being analyzed.

6.4 IceCube, the Facility

During its construction phase, IceCube demonstrated a significant potential for facilitating a range of other research. For example, a dust logger provided measurements with millimeter precision that are valuable for event reconstruction in IceCube but that also provide a record of surface winds over more than 100,000 years [138].

Already during construction of AMANDA, antennas forming the RICE detector were deployed in some holes to expand the target volume in the search for cosmogenic neutrinos [139]. An acoustic test setup of receivers in the upper portion of four IceCube holes was deployed in 2007 to explore the acoustic technique for detecting ultra-high-energy neutrinos. A retrievable transmitter (pinger) was submerged briefly in several newly prepared holes at various depths and distances from the receivers to measure the attenuation of sound in ice. The attenuation length of 300 m is significantly less than had been expected [140]. The Askaryan Radio Array (ARA) [141] plans to take advantage of the kilometer-scale attenuation for radio signals in ice to construct a detector with a 200 km^2 effective area, which should be sufficient to determine the level of production of cosmogenic neutrinos, which at present is highly uncertain. The initially deployed ARA detectors send data to computers housed in the ICL for staging and transmission to the north.

The DM-Ice experiment [142] proposes to repeat the DAMA experiment in the quiet environment of the Antarctic ice. An interesting feature of the

observation is the fact that the seasonal modulation of the muon rate has the opposite phase relative to the motion of the Earth through the gas of dark matter as compared to a detector in the Northern Hemisphere. A test detector to explore the noise environment for DM-Ice was deployed at the bottom of an IceCube string in December 2010. Its computers and data transmission are also hosted in the ICL.

The enhancement of the low-energy capabilities of IceCube provided by the DeepCore subarray has led to the PINGU proposal [143] to deploy an additional 40 strings within the existing DeepCore detector. This would lower the threshold to below 5 GeV ($<$ 25 m muon track length in ice). In this energy range, matter effects in the Earth lead to resonant oscillations of $\nu_\mu \leftrightarrow \nu_e$ ($\bar{\nu}_\mu \leftrightarrow \bar{\nu}_e$) for normal (inverted) hierarchy [144] that depend on zenith angle. By taking advantage of the fact that the neutrino cross section is larger than that for antineutrinos, coupled with the excess of ν_μ compared to $\bar{\nu}_\mu$, a measurement sensitive to the neutrino mass hierarchy is possible on a relatively short time scale. PINGU would also have sensitivity to ν_μ disappearance, ν_τ appearance, and maximal mixing. The lower energy threshold would also enhance the indirect searches for dark matter with IceCube as well as the sensitivity to neutrinos from supernova explosions. In addition, there is the potential for neutrino tomography of the Earth with PINGU.

The observation of extraterrestrial neutrinos up to the PeV range has stimulated ideas to enhance the discovery potential in that area. One possibility is to improve the atmospheric neutrino veto by expanding the surface array [145]. Expansion of the existing array with strings deployed at a larger separation is also possible in the long term.

7 Future Developments

7.1 IceCube-Gen2: from Discovery to Astronomy

By building IceCube, it was possible to map the optical properties of natural ice over large distances. We made the surprising discovery that the absorption length of the Cherenkov light to which the photomultipliers are sensitive exceeds 100 m. In fact, in the lower half of the detector, it exceeds 200 m. The absorption length dictates the distance by which one can space the strings of sensors without spoiling the uniformity of the detector. Current modeling indicates that spacings of 250 m, possibly larger, are acceptable. One can therefore instrument a ten-times-larger volume of ice with the same number of strings used to build IceCube. The design of such a next-generation instrument using superior light sensors and data acquisition electronics is in progress [146]. IceCube-Gen2 will turn a fascinating discovery into an instrument for neutrino astronomy.

The larger spacings do of course result in a higher threshold but this is not necessarily bad. While the 100,000 or so atmospheric neutrinos that IceCube collects above a threshold of 100 GeV every year were useful for calibration, they represent a severe background for isolating the cosmic component of the

flux. The peak sensitivity to an E^{-2} spectrum is reached at 40 TeV [60, 61]. While the detector has to be efficient below that energy, a threshold much lower than this value introduces background without a gain in signal. Designs for a next-generation instrument are in progress [146].

As discussed in the previous sections, the absence of a strong anisotropy of neutrino arrival directions raises the possibility that the cosmic neutrinos originate from a number of relatively weak extragalactic sources. It is indeed important to keep in mind that the interaction rate of a neutrino is so low that it travels unattenuated over cosmic distances through the tenuous matter and radiation backgrounds of the Universe. This makes the identification of individual point sources contributing to the IceCube flux challenging [147, 148, 149, 102]. Even so, it is also important to realize that IceCube is capable of localizing the sources by observing multiple neutrinos originating in the same location. Not having observed neutrino clusters in the present data raises the question of how many events are required to make such a model-independent identification possible. The answer to this question suggests the construction of a next-generation detector that instruments a ten times larger volume of ice [146].

Following the analysis of Ref. [102], let's estimate the number of cosmic neutrinos required to detect a spatial cluster of m, or more, neutrino events from the same source. The observed cluster will most likely come from a nearby source and we can hence simplify the calculation by considering Euclidean space. The number of events $n(r)$ from a local source at a distance $r \leq H_0^{-1}$, i.e., smaller than the Hubble radius, is

$$n(r) \simeq \frac{H_0}{f_{\rm sky} 4\pi r^2 \xi_z} \times \frac{N}{\rho_0} \tag{54}$$

Here, N is the number of events from all sources with a local density ρ_0 and, as before, the cosmological evolution of the sources is parametrized by an effective parameter ξ_z. For instance, assuming that the cosmic-ray sources track star formation, then $\xi_z \simeq 2.4$. The local Hubble constant H_0 sets the effective size, c/H_0, of the observable Universe (and in this way solves the neutrino variant of Olbers' paradox for infinite homogeneous neutrino source distributions). Finally, $f_{\rm sky}$ is the sky coverage of the detector in units of 4π.

As a back-of-the-envelope estimate of the total number of events required for the observation of event multiplets, we consider the contribution of the closest source expected in the field of view (FoV) within a sphere of volume $V_1 = 1/(f_{\rm sky}\rho_0)$. The total number of events that we expect from this volume is given by the integral of Eq. 54 over V_1 and yields $m = N(V_1/V_H)^{\frac{1}{3}}/\xi_z$ where we introduce the Hubble volume $V_H = 4\pi/(3H_0^3)$. Note that V_H/V_1 corresponds to the effective number of sources in the FoV. In the case of continuous sources, we arrive then at an expected total for m local events of

$$N \simeq 740 \left(\frac{m}{2}\right) \xi_{z,2.4} \left(f_{\rm sky}\, \rho_{0,-5}\right)^{\frac{1}{3}} . \tag{55}$$

Therefore, to observe a cluster of events from the nearest source requires

a sample on the order of $1,000$ neutrinos for a local source density of $\rho_0 = 10^{-5}\mathrm{Mpc}^{-3}$, the characteristic local density of AGNs. Other source candidates may have larger or smaller densities, but notice that the dependence of the number of events required on the density is relatively weak, $\propto \rho_0^{1/3}$. Still, it will realistically require a sample of more than a thousand neutrino events with good angular resolution and little background to identify the sources. This would take roughly 20 years or so with the present instrument. An instrument with 5–10 times the sensitivity of IceCube is required to operate as an effective telescope collecting a thousand events in a few years. Detailed calculations that take into account ensemble variations of the source distribution as well as the event statistics of individual sources can be found in Ref. [102].

A higher signal-to-background ratio can be achieved if the observed events are variable in time, typical for extragalactic sources [102]. In the case of transient sources, we have to take into account that the number of sources is increasing with observation time $T_{\mathrm{live}} = N/\dot{N}$. Solving in terms of the total observation rate $\dot{N}$ we arrive at

$$N \simeq 637 \left(\frac{m}{2}\right)^{\frac{3}{2}} \xi_{z,2.4}^{\frac{3}{2}} \left(f_{\mathrm{sky}} \dot{\rho}_{0,-6}/\dot{N}_2\right)^{\frac{1}{2}} , \tag{56}$$

with an event rate $\dot{N} = 100\dot{N}_2/\mathrm{yr}$. In the case of rare transient sources like long-duration GRBs with (isotropic equivalent) rate density of $\dot{\rho}_0 \simeq 10^{-9}\mathrm{Mpc}^{-3}\,\mathrm{yr}^{-1}$ [150], an identification of the sources with IceCube itself is still likely.

Significantly fewer events are required to identify the source population if the observed events can be correlated with astronomical catalogues [102]. In fact, a recent study looking for the combined neutrino emission of Fermi identified blazars [107] could place upper limits on their contribution to the IceCube observation at the level of 30%. A related population study has recently been carried out in Ref. [151]. Also, the contribution of GRBs to the diffuse emission is limited to less than 10% due to strong IceCube limits on the prompt neutrino emission of GRBs coincidence with the gamma-ray display [152].

Despite the degraded resolution and the reduced potential for astronomy, the observation of electron and tau neutrinos should still be a priority. They complement the sky coverage of muon neutrinos that, at PeV energy, are mostly detected near the horizon because they are absorbed by the Earth. At high energies, neutrino production can happen in the production and decay of unstable nuclei, e.g., neutrons with $n \to pe^-\bar{\nu}_e$ or mesons, e.g., $\pi^+ \to \mu^+\nu_\mu$. Note that the neutrino production from the decay of muons $\mu^+ \to e^+\nu_e\bar{\nu}_\mu$ can be suppressed relative to the pion decay channel if synchrotron losses are important. Hence, the flavor composition is likely energy dependent and provides insight into the relative energy loss of high-energy pions and muons in the magnetic field of the cosmic accelerator [153].

Various authors have studied the implications of IceCube's HESE (high-energy starting event) topologies with astrophysical and/or exotic production mechanisms [155, 156, 157, 158, 159, 160, 161, 162]. Figure 20 shows the general neutrino flavor phase space ν_e:ν_μ:ν_τ and the expected intrinsic flavor ratio in astrophysical sources from neutron decay (triangle), pion+muon decay (circle),

and muon-damped pion decay (square). The observable neutrino flavor ratio is expected to be averaged over many oscillations. This leaves only a very narrow range for the possible flavor composition, which is shown as the line in the center of Fig. 20. The corresponding observable flavor ratios of the three astrophysical production mechanisms are also indicated. The final parameter space is very close to the "tri-bi-maximal" approximation of mixing angles, which predicts that the final flavor ratio depends only on the initial electron neutrino ratio $x = N_{\nu_e}/N_{\nu_{\rm tot}}$ and $(2/3 + x)$:$(7/6 - x/2)$:$(7/6 - x/2)$.

The precise relation between HESE topologies and flavor composition is non-trivial, since atmospheric backgrounds and detector effects have to be taken into account properly. In a recent IceCube analysis [103], it was shown that the observation of tracks and cascades is consistent with most astrophysical scenarios within uncertainties. At sub-PeV energies (before ν_τ events can be distinguished from single cascades), the observation is mostly degenerate in terms of the total $\nu_e + \nu_\tau$ ratio, except for the contribution of prompt tau decays into muons. The expected fraction for tracks out of the total number events is about $7/24 - x/8$, where we take into account that CC interactions are about three times larger than neutral current interactions at these energies. The uncertainty of the inferred intrinsic electron-neutrino fraction x is hence about eight times higher than the uncertainty of the track fraction. The situation becomes even more challenging if we include backgrounds and systematic uncertainties.

The situation of flavor identification improves at super-PeV neutrino energies. On one hand, the decay length of the τ produced in CC ν_τ interactions becomes resolvable by the detector and can in principle be distinguished from tracks and cascade events as argued before. On the other hand, electron antineutrinos, $\bar{\nu}_e$, can resonantly interact with in-ice electrons via the Glashow resonance, $\bar{\nu}_e e^- \to W^-$, at neutrino energies of about 6.3 PeV. This could be observable as a peak in the cascade spectrum, depending on the relative contribution of $\bar{\nu}_e$ after oscillation. In principle, this will allow us to answer the basic question of whether the cosmic neutrinos are photo- or hadro-produced in the source with different neutrino-to-antineutrino ratios [163, 164].

Construction of a next-generation instrument with at least five times higher sensitivity would likely result in the observation of cosmogenic neutrinos [146]. The rate expected with IceCube currently is only one event per year, assuming that all cosmic rays are protons (and it is difficult to imagine that a significant component of the highest energy neutrinos would not be protons). Obviously, higher sensitivity would also benefit the wide range of measurements performed with the present detector, from the search for dark matter to the precision limits on any violation of Lorentz invariance.

7.2 Future Water-Based Detectors: KM3NeT and GVD

Accelerators of cosmic rays produce neutrino fluxes limited in energy to roughly 5% of the maximal energy of the protons or nuclei (see Eq. 4). For Galactic neutrino sources, even the as yet unidentified PeVatrons, we thus expect neu-

trino spectra with a cutoff (see Eq. 32) in the range between a few and roughly 100 TeV. Detection of these neutrinos requires optimized sensitivities in the TeV range. In particular, the atmospheric muon background limits the field of view of neutrino telescopes to the downward hemisphere at these energies.

With IceCube focusing on high energies, a second, kilometer-scale neutrino telescope in the Northern Hemisphere is therefore necessary to observe the Galactic center and the largest part of the Galactic plane—or, more generally speaking, to grant full-sky coverage for neutrino astronomy. The sky coverage in Galactic coordinates of IceCube and a Mediterranean-based telescope is indicated in Fig. 21.

Following up the pioneering work of DUMAND, several neutrino telescope projects were initiated in the Mediterranean in the 1990s. In 2008, the construction of the ANTARES detector off the French coast near Toulon was completed. With an instrumented volume of a percent of a cubic kilometer, ANTARES [165] has about the same effective area as AMANDA and is currently the most sensitive observatory for high-energy neutrinos in the Northern Hemisphere. It has demonstrated the feasibility of neutrino detection in the deep sea and has provided a wealth of technical experience and design solutions for deep-sea components.

The next step will be the construction of a multi-cubic-kilometer neutrino telescope in the Mediterranean Sea, KM3NeT. Its technical design [166] has been elaborated in EU-funded projects[2]. Major progress has been made, in particular concerning the reliability and the cost-effectiveness of the design. A prime example of the many new technical developments is the digital optical module, which incorporates 31 3-inch photomultipliers instead of one large tube (see Fig. 22). The advantages are a tripling of the photocathode area per optical module, a segmentation of the photocathode allowing for a clean identification of coincident Cherenkov photons, some directional sensitivity, and a reduction of the overall number of penetrators and connectors, which are expensive and failure-prone. For all photomultiplier signals exceeding the noise level, time-over-threshold information will be digitized and time-stamped by electronic modules housed inside the optical modules. This information will be sent via optical fibers to shore, where the data stream will be filtered online for event candidates.

KM3NeT in its initial phase will consist of 110 vertical structures (detection units) carrying more than 10,000 optical modules. The detection units are anchored to the seabed with deadweights and kept vertical by submerged buoys. The vertical distances between optical modules will be about 40 m, the horizontal distances between detection units will be about 100 m, depending on the outcome of ongoing optimization studies. The detector will be built near Capo Passero (East of Sicily).

Due to the drag of deep-sea currents, the detection units will deform and deviate horizontally by up to several tens of meters from their nominal vertical arrangement. Acoustic triangulation, tiltmeters, and compasses will be used to

[2]FP6 Design Study and FP7 Preparatory Phase

monitor the position and orientation of each optical module with a precision commensurate with a timing resolution of 1 ns.

A parallel effort is underway in Lake Baikal with the deep underwater neutrino telescope Baikal-GVD (Gigaton Volume Detector). The first GVD cluster, named DUBNA, has been upgraded in March and April 2016 to its final size (288 optical modules, diameter 120 m, height 525 m, and instrumented volume of 6 Mt). Each of the eight strings consists of three sections with 12 optical modules. Deployment of a second cluster is foreseen for spring 2017.

8 Acknowledgements

I thank my IceCube collaborators for discussions and M. Ahlers, A. Kheirandish and Logan Wille for a critical reading of the manuscript. This research was supported in part by the U.S. National Science Foundation under Grants No. OPP-0236449 and PHY-0354776; by the U.S. Department of Energy under Grant No. DE-FG02-95ER40896; by the University of Wisconsin Research Committee with funds granted by the Wisconsin Alumni Research Foundation.

References

[1] Reines F and Cowan C L 1956 *Nature* **178** 446–449

[2] Halzen F and Klein S R 2008 *Phys. Today* **61N5** 29–35

[3] Roberts A 1992 *Rev.Mod.Phys.* **64** 259–312

[4] Gaisser T K, Halzen F and Stanev T 1995 *Phys.Rept.* **258** 173–236 (*Preprint* `hep-ph/9410384`)

[5] Learned J and Mannheim K 2000 *Ann.Rev.Nucl.Part.Sci.* **50** 679–749

[6] Halzen F and Hooper D 2002 *Rept.Prog.Phys.* **65** 1025–1078 (*Preprint* `astro-ph/0204527`)

[7] Markov M 1960 *Proc. of the 10th Intl. Conf. on High-Energy Physics* 578–581

[8] Babson J *et al.* (DUMAND Collaboration) 1990 *Phys.Rev.* **D42** 3613–3620

[9] Balkanov V *et al.* (BAIKAL collaboration) 2003 *Nucl.Phys.Proc.Suppl.* **118** 363–370

[10] Aggouras G *et al.* (NESTOR Collaboration) 2005 *Astropart.Phys.* **23** 377–392

[11] Aguilar J *et al.* (ANTARES Collaboration) 2006 *Astropart.Phys.* **26** 314–324 (*Preprint* `astro-ph/0606229`)

[12] Migneco E 2008 *J.Phys.Conf.Ser.* **136** 022048

[13] IceCube Collaboration 2001 Icecube preliminary design document http://www.icecube.wisc.edu/science/publications/pdd/pdd.pdf

[14] Ahrens J *et al.* (IceCube Collaboration) 2004 *Astropart.Phys.* **20** 507–532 (*Preprint* astro-ph/0305196)

[15] Becker J K 2008 *Phys.Rept.* **458** 173–246 (*Preprint* 0710.1557)

[16] Achterberg A *et al.* (IceCube) 2007 *Phys. Rev.* **D76** 042008 [Erratum: Phys. Rev.D77,089904(2008)] (*Preprint* 0705.1315)

[17] Rhode W *et al.* (Frejus) 1996 *Astropart. Phys.* **4** 217–225

[18] Engel R, Seckel D and Stanev T 2001 *Phys.Rev.* **D64** 093010 (*Preprint* astro-ph/0101216)

[19] Sommers P 2012 *Astropart. Phys.* **39-40** 88–94

[20] Particle Data Group URL pdg.lbl.gov

[21] Baade W and Zwicky F 1934 *Proceedings of the National Academy of Science* **20** 259–263

[22] HESS Collaboration 2016 *Nature* **531** 476–479

[23] Ginzburg V L and Syrovatskii S I 1969 *The origin of cosmic rays*

[24] Butt Y 2009 *Nature* **460** 659–772 (*Preprint* 1009.3664)

[25] Gaisser T K 2001 *AIP Conf.Proc.* **558** 27–42 (*Preprint* astro-ph/0011524)

[26] Waxman E 1995 *Phys. Rev. Letters* **75** 386

[27] Gonzalez-Garcia M, Maltoni M and Rojo J 2006 *JHEP* **0610** 075 (*Preprint* hep-ph/0607324)

[28] Daum K *et al.* (Frejus Collaboration.) 1995 *Z.Phys.* **C66** 417–428

[29] Abbasi R *et al.* (IceCube Collaboration) 2009 *Phys.Rev.* **D79** 102005 (*Preprint* 0902.0675)

[30] Abbasi R *et al.* (IceCube Collaboration) 2010 *Astropart.Phys.* **34** 48–58 (*Preprint* 1004.2357)

[31] Abbasi R *et al.* (IceCube Collaboration) 2011 *Phys.Rev.* **D83** 012001 (*Preprint* 1010.3980)

[32] Abbasi R *et al.* (IceCube Collaboration) 2011 *Phys.Rev.* **D84** 082001 (*Preprint* 1104.5187)

[33] Aartsen M *et al.* (IceCube) 2013 *Phys.Rev.Lett.* **110** 151105 (*Preprint* 1212.4760)

[34] Honda M, Kajita T, Kasahara K, Midorikawa S and Sanuki T 2007 *Phys.Rev.* **D75** 043006 (*Preprint* astro-ph/0611418)

[35] Barr G, Gaisser T, Lipari P, Robbins S and Stanev T 2004 *Phys.Rev.* **D70** 023006 (*Preprint* astro-ph/0403630)

[36] Enberg R, Reno M H and Sarcevic I 2008 *Phys.Rev.* **D78** 043005 (*Preprint* 0806.0418)

[37] Aartsen M G *et al.* (IceCube) 2016 *Astrophys. J.* **824** 115 (*Preprint* 1601.06484)

[38] Berezhko E 2008 *Astrophys.J.* **684** L69–L71 (*Preprint* 0809.0734)

[39] Becker Tjus J, Eichmann B, Halzen F, Kheirandish A and Saba S M 2014 *Phys. Rev.* **D89** 123005 (*Preprint* 1406.0506)

[40] Hooper D 2016 *JCAP* **1609** 002 (*Preprint* 1605.06504)

[41] Gaisser T 1997 (*Preprint* astro-ph/9707283)

[42] Ahlers M, Anchordoqui L A, Goldberg H, Halzen F, Ringwald A *et al.* 2005 *Phys.Rev.* **D72** 023001 (*Preprint* astro-ph/0503229)

[43] Abbasi R *et al.* (IceCube) 2011 *Astrophys.J.* **732** 18 (*Preprint* 1012.2137)

[44] Wakely S and Horan D Tevcat, an online gamma-ray catalog URL http://tevcat.uchicago.edu/

[45] Alvarez-Muniz J and Halzen F 2002 *Astrophys.J.* **576** L33–L36 (*Preprint* astro-ph/0205408)

[46] Becker J K, Halzen F, O'Murchadha A and Olivo M 2010 (*Preprint* 1003.4710)

[47] Gaisser T K 2013 *EPJ Web Conf.* **53** 01012

[48] Halzen F 2013 *Riv.Nuovo Cim.* **36** 81–104

[49] Mannheim K and Schlickeiser R 1994 *Astron. Astrophys.* **286** 983–996 (*Preprint* astro-ph/9402042)

[50] Kelner S R, Aharonian F A and Bugayov V V 2006 *Phys. Rev.* **D74** 034018 [Erratum: Phys. Rev.D79,039901(2009)] (*Preprint* astro-ph/0606058)

[51] Wang X and Loeb A 2016 (*Preprint* 1607.06476)

[52] Halzen F and Kheirandish A 2016 (*Preprint* 1605.06119)

[53] Gonzalez-Garcia M, Halzen F and Mohapatra S 2009 *Astropart.Phys.* **31** 437–444 (*Preprint* 0902.1176)

[54] Ahlers M, Mertsch P and Sarkar S 2009 *Phys. Rev.* **D80** 123017 (*Preprint* 0909.4060)

[55] Abdo A A *et al.* 2007 *Astrophys. J.* **658** L33–L36 (*Preprint* astro-ph/0611691)

[56] Halzen F, Kheirandish A and Niro V 2016 (*Preprint* 1609.03072)

[57] Gabici S and Aharonian F A 2007 *Astrophys. J.* **665** L131 (*Preprint* 0705.3011)

[58] Ackermann M *et al.* (Fermi-LAT) 2013 *Science* **339** 807 (*Preprint* 1302.3307)

[59] Abdo A A (Fermi-LAT) 2011 *Astrophys. J.* **734** 28 (*Preprint* 1103.5727)

[60] Halzen F, Kappes A and O'Murchadha A 2008 *Phys.Rev.* **D78** 063004 (*Preprint* 0803.0314)

[61] Kappes A, Halzen F and O Murchadha A 2009 *Nucl. Instrum. Meth.* **A602** 117–119

[62] Waxman E and Bahcall J N 1997 *Phys.Rev.Lett.* **78** 2292–2295 (*Preprint* astro-ph/9701231)

[63] Guetta D, Hooper D, Alvarez-Muniz J, Halzen F and Reuveni E 2004 *Astropart. Phys.* **20** 429–455 (*Preprint* astro-ph/0302524)

[64] Hummer S, Baerwald P and Winter W 2012 *Phys. Rev. Lett.* **108** 231101 (*Preprint* 1112.1076)

[65] Ahlers M, Gonzalez-Garcia M C and Halzen F 2011 *Astropart. Phys.* **35** 87–94 (*Preprint* 1103.3421)

[66] Abbasi R *et al.* (IceCube Collaboration) 2011 *Phys.Rev.* **D83** 092003 (*Preprint* 1103.4250)

[67] Senno N, Murase K and Meszaros P 2016 *Phys. Rev.* **D93** 083003 (*Preprint* 1512.08513)

[68] Bottcher M and Dermer C D 1998 *Astrophys. J.* **499** L131–L134 (*Preprint* astro-ph/9801027)

[69] Ahlers M, Anchordoqui L, Gonzalez-Garcia M, Halzen F and Sarkar S 2010 *Astropart.Phys.* **34** 106–115 (*Preprint* 1005.2620)

[70] Abdo A A *et al.* (Fermi-LAT) 2010 *Phys. Rev. Lett.* **104** 101101 (*Preprint* 1002.3603)

[71] Aartsen M G *et al.* (IceCube) 2016 (*Preprint* 1607.05886)

[72] Ulrich R, Engel R, Muller S, Schussler F and Unger M 2009 *Nucl. Phys. Proc. Suppl.* **196** 335–340 (*Preprint* 0906.3075)

[73] Kotera K, Allard D and Olinto A 2010 *JCAP* **1010** 013 (*Preprint* 1009.1382)

[74] Murase K, Inoue Y and Dermer C D 2014 *Phys. Rev.* **D90** 023007 (*Preprint* 1403.4089)

[75] Aab A *et al.* (Pierre Auger) 2015 *Phys. Rev.* **D91** 092008 (*Preprint* 1504.05397)

[76] Gorham P W *et al.* (ANITA) 2010 *Phys. Rev.* **D82** 022004 [Erratum: Phys. Rev.D85,049901(2012)] (*Preprint* 1011.5004)

[77] Spiering C 2008 High energy neutrino astronomy: Status and perspectives vol 1085 pp 18–29 URL http://scitation.aip.org/content/aip/proceeding/aipcp/10.1063/1.3076635

[78] Katz U and Spiering C 2012 *Prog.Part.Nucl.Phys.* **67** 651–704 (*Preprint* 1111.0507)

[79] Halzen F and Klein S R 2010 *Rev. Sci. Instrum.* **81** 081101 (*Preprint* 1007.1247)

[80] Halzen F 2006 *Eur. Phys. J.* **C46** 669–687 (*Preprint* astro-ph/0602132)

[81] KM3NeT Coll URL http://www.km3net.org/

[82] Halzen F and Saltzberg D 1998 *Phys. Rev. Lett.* **81** 4305–4308 (*Preprint* hep-ph/9804354)

[83] Middell E 2011 Search for atmospheric neutrino induced particle showers with IceCube 40 *Proceedings, 32nd International Cosmic Ray Conference (ICRC 2011): Beijing, China, August 11-18, 2011* vol 4 pp 246–249 URL http://www.ihep.ac.cn/english/conference/icrc2011/paper/proc/v4/v4_1097.pdf

[84] Klein S R 2004 Cascades from nu(E) above 10**20 eV *INFN Eloisatron Project 44th Workshop on QCD at Cosmic Energies: The Highest Energy Cosmic Rays and QCD Erice, Italy, August 29-September 5, 2004* (*Preprint* astro-ph/0412546)

[85] Learned J G and Pakvasa S 1995 *Astropart.Phys.* **3** 267–274 (*Preprint* hep-ph/9405296)

[86] Schönert S, Gaisser T K, Resconi E and Schulz O 2009 *Phys.Rev.* **D79** 043009 (*Preprint* 0812.4308)

[87] Gaisser T K, Stanev T and Tilav S 2013 *Front. Phys.(Beijing)* **8** 748–758 (*Preprint* 1303.3565)

[88] Aglietta M *et al.* (LVD Collaboration) 1999 *Phys.Rev.* **D60** 112001 (*Preprint* hep-ex/9906021)

[89] Schukraft A (IceCube Collaboration) 2013 *Nucl.Phys.Proc.Suppl.* **237-238** 266–268 (*Preprint* 1302.0127)

[90] Gaisser T K 2013 *EPJ Web Conf.* **52** 09004 (*Preprint* 1303.1431)

[91] Desiati P and Gaisser T K 2010 *Phys. Rev. Lett.* **105** 121102 (*Preprint* 1008.2211)

[92] Ahrens J *et al.* (AMANDA Collaboration) 2004 *Nucl.Instrum.Meth.* **A524** 169–194 (*Preprint* astro-ph/0407044)

[93] Aartsen M *et al.* (IceCube Collaboration) 2014 *JINST* **9** P03009 (*Preprint* 1311.4767)

[94] Kopper C, Giang W and Kurahashi N 2015 Observation of Astrophysical Neutrinos in Four Years of IceCube Data Proceedings of ICRC2015 **1081**

[95] Schoenen S and Rädel L 2015 *Proceedings of ICRC2015* **1079** 642

[96] Aartsen M G *et al.* (IceCube) 2015 *Phys. Rev. Lett.* **115** 081102 (*Preprint* 1507.04005)

[97] Weaver C 2014 Icecube results for diffuse muon neutrinos APS April Meeting 2014, Savannah, Georgia, USA

[98] Aartsen M *et al.* (IceCube Collaboration) 2013 *Phys.Rev.Lett.* **111** 021103 (*Preprint* 1304.5356)

[99] Gaisser T K, Jero K, Karle A and van Santen J 2014 *Phys.Rev.* **D90** 023009 (*Preprint* 1405.0525)

[100] Aartsen M *et al.* (IceCube Collaboration) 2014 *Phys.Rev.* **D89** 102001 (*Preprint* 1312.0104)

[101] Aartsen M *et al.* (IceCube Collaboration) 2014 *Phys.Rev.Lett.* **113** 101101 (*Preprint* 1405.5303)

[102] Ahlers M and Halzen F 2014 *Phys. Rev.* **D90** 043005 (*Preprint* 1406.2160)

[103] Aartsen M G *et al.* (IceCube) 2015 *Phys. Rev. Lett.* **114** 171102 (*Preprint* 1502.03376)

[104] Aartsen M G *et al.* (IceCube) 2015 *Phys. Rev.* **D91** 022001 (*Preprint* 1410.1749)

[105] Ackermann M *et al.* (Fermi-LAT) 2015 *Astrophys. J.* **799** 86 (*Preprint* 1410.3696)

[106] Murase K, Ahlers M and Lacki B C 2013 *Phys.Rev.* **D88** 121301 (*Preprint* 1306.3417)

[107] Glüsenkamp T (IceCube) 2015 (*Preprint* 1502.03104)

[108] Padovani P and Resconi E 2014 *Mon.Not.Roy.Astron.Soc.* **443** 474–484 (*Preprint* 1406.0376)

[109] Padovani P, Resconi E, Giommi P, Arsioli B and Chang Y L 2016 *Mon. Not. Roy. Astron. Soc.* **457** 3582–3592 (*Preprint* 1601.06550)

[110] Krauß F *et al.* 2014 *Astron. Astrophys.* **566** L7 (*Preprint* 1406.0645)

[111] Kadler M *et al.* 2016 (*Preprint* 1602.02012)

[112] Feldstein B, Kusenko A, Matsumoto S and Yanagida T T 2013 *Phys.Rev.* **D88** 015004 (*Preprint* 1303.7320)

[113] Esmaili A and Serpico P D 2013 *JCAP* **1311** 054 (*Preprint* 1308.1105)

[114] Bai Y, Lu R and Salvado J 2016 *JHEP* **01** 161 (*Preprint* 1311.5864)

[115] Bhattacharya A, Reno M H and Sarcevic I 2014 *JHEP* **1406** 110 (*Preprint* 1403.1862)

[116] Esmaili A, Kang S K and Serpico P D 2014 *JCAP* **1412** 054 (*Preprint* 1410.5979)

[117] Cherry J F, Friedland A and Shoemaker I M 2014 *JCAP* (*Preprint* 1411.1071)

[118] Murase K, Laha R, Ando S and Ahlers M 2015 *Phys. Rev. Lett.* **115** 071301 (*Preprint* 1503.04663)

[119] Esmaili A and Serpico P D 2015 *JCAP* **1510** 014 (*Preprint* 1505.06486)

[120] Aartsen M *et al.* (IceCube collaboration) 2013 *Phys.Rev.Lett.* **110** 131302 (*Preprint* 1212.4097)

[121] Abbasi R *et al.* (IceCube Collaboration) 2011 *Phys.Rev.* **D84** 022004 (*Preprint* 1101.3349)

[122] Abbasi R *et al.* (IceCube) 2012 (*Preprint* 1210.3557)

[123] Aartsen M *et al.* (IceCube Collaboration) 2013 *Phys.Rev.* **D88** 122001 (*Preprint* 1307.3473)

[124] Rameez M and (for the IceCube Collaboration) T M 2015 *PoS* **ICRC2015**

[125] (for the IceCube Collaboration) M Z 2015 *PoS* **ICRC2015**

[126] Gondolo P, Edsjo J, Ullio P, Bergstrom L, Schelke M and Baltz E A 2004 *JCAP* **0407** 008 (*Preprint* astro-ph/0406204)

[127] Ullio P, Kamionkowski M and Vogel P 2001 *JHEP* **07** 044 (*Preprint* hep-ph/0010036)

[128] Choi K *et al.* (Super-Kamiokande) 2015 *Phys. Rev. Lett.* **114** 141301 (*Preprint* 1503.04858)

[129] Tönnis C *et al.* 2015 *PoS* **ICRC2015**

[130] Amole C *et al.* (PICO) 2015 *Phys. Rev. Lett.* **114** 231302 (*Preprint* 1503.00008)

[131] Savage C, Gelmini G, Gondolo P and Freese K 2009 *JCAP* **0904** 010 (*Preprint* 0808.3607)

[132] Aalseth C E *et al.* 2011 *Phys. Rev. Lett.* **107** 141301 (*Preprint* 1106.0650)

[133] Agnese R *et al.* (CDMS) 2013 *Phys. Rev. Lett.* **111** 251301 (*Preprint* 1304.4279)

[134] Aartsen M G *et al.* (IceCube) 2013 *Phys. Rev. Lett.* **111** 081801 (*Preprint* 1305.3909)

[135] Fogli G L, Lisi E, Marrone A, Montanino D, Palazzo A and Rotunno A M 2012 *Phys. Rev.* **D86** 013012 (*Preprint* 1205.5254)

[136] Abbasi R *et al.* (IceCube Collaboration) 2011 *Astron.Astrophys.* **535** A109 (*Preprint* 1108.0171)

[137] Abbasi R *et al.* (IceCube) 2008 *Astrophys. J.* **689** L65–L68 (*Preprint* 0810.2034)

[138] Bay R C, Rohde R A, Price P B and Bramall N E 2010 *Journal of Geophysical Research: Atmospheres* **115** n/a–n/a ISSN 2156-2202 d14126 URL http://dx.doi.org/10.1029/2009JD013741

[139] Kravchenko I, Hussain S, Seckel D, Besson D, Fensholt E, Ralston J, Taylor J, Ratzlaff K and Young R 2012 *Phys. Rev.* **D85** 062004 (*Preprint* 1106.1164)

[140] Abbasi R *et al.* (IceCube) 2011 *Astropart. Phys.* **34** 382–393 (*Preprint* 1004.1694)

[141] Allison P, Auffenberg J, Bard R, Beatty J, Besson D *et al.* 2012 *Astropart.Phys.* **35** 457–477 (*Preprint* 1105.2854)

[142] Cherwinka J *et al.* 2012 *Astropart. Phys.* **35** 749–754 (*Preprint* 1106.1156)

[143] The IceCube-Gen2 Collaboration PINGU LOI

[144] Akhmedov E K, Razzaque S and Smirnov A Yu 2013 *JHEP* **02** 082 [Erratum: JHEP07,026(2013)] (*Preprint* 1205.7071)

[145] Aartsen M G *et al.* (IceCube) 2013 The IceCube Neutrino Observatory Part VI: Ice Properties, Reconstruction and Future Developments *Proceedings, 33rd International Cosmic Ray Conference (ICRC2013): Rio de Janeiro, Brazil, July 2-9, 2013* (*Preprint* 1309.7010) URL http://inspirehep.net/record/1255632/files/arXiv:1309.7010.pdf

[146] Aartsen M *et al.* (IceCube Collaboration) 2014 (*Preprint* 1412.5106)

[147] Lipari P 2006 *Nucl.Instrum.Meth.* **A567** 405–417 (*Preprint* astro-ph/0605535)

[148] Becker J K, Groß A, Münich K, Dreyer J, Rhode W and Biermann P L 2007 *Astropart.Phys.* **28** 98–118 (*Preprint* astro-ph/0607427)

[149] Silvestri A and Barwick S W 2010 *Phys.Rev.* **D81** 023001 (*Preprint* 0908.4266)

[150] Wanderman D and Piran T 2010 *Mon.Not.Roy.Astron.Soc.* **406** 1944–1958 (*Preprint* 0912.0709)

[151] Wang B and Li Z 2015 (*Preprint* 1505.04418)

[152] Abbasi R *et al.* (IceCube Collaboration) 2012 *Nature* **484** 351–353 (*Preprint* 1204.4219)

[153] Kashti T and Waxman E 2005 *Phys.Rev.Lett.* **95** 181101 (*Preprint* astro-ph/0507599)

[154] Gonzalez-Garcia M, Maltoni M, Salvado J and Schwetz T 2012 *JHEP* **1212** 123 (*Preprint* 1209.3023)

[155] Mena O, Palomares-Ruiz S and Vincent A C 2014 *Phys.Rev.Lett.* **113** 091103 (*Preprint* 1404.0017)

[156] Fu L and Ho C M 2014 (*Preprint* 1407.1090)

[157] 2014 (*Preprint* 1410.0408)

[158] Fu L, Ho C M and Weiler T J 2014 (*Preprint* 1411.1174)

[159] Xu X J, He H J and Rodejohann W 2014 *JCAP* **1412** 039 (*Preprint* 1407.3736)

[160] Palomares-Ruiz S, Mena O and Vincent A C 2014 (*Preprint* 1411.2998)

[161] Palladino A, Pagliaroli G, Villante F and Vissani F 2015 *Phys.Rev.Lett.* **114** 171101 (*Preprint* 1502.02923)

[162] Palladino A and Vissani F 2015 (*Preprint* 1504.05238)

[163] Anchordoqui L A, Goldberg H, Halzen F and Weiler T J 2005 *Phys.Lett.* **B621** 18–21 (*Preprint* hep-ph/0410003)

[164] Winter W 2013 *Phys.Rev.* **D88** 083007 (*Preprint* 1307.2793)

[165] M Ageron et al and ANTARES Coll 2011 *Nucl. Instrum. Meth* **A 656** 11 (*Preprint* astro-ph.IM/1104.1607) URL http://antares.in2p3.fr/

[166] P Bagley et al and KM3NeT Coll 2010 "KM3NeT Technical Design Report" Tech. rep. URL http://www.km3net.org/TDR/TDRKM3NeT.pdf

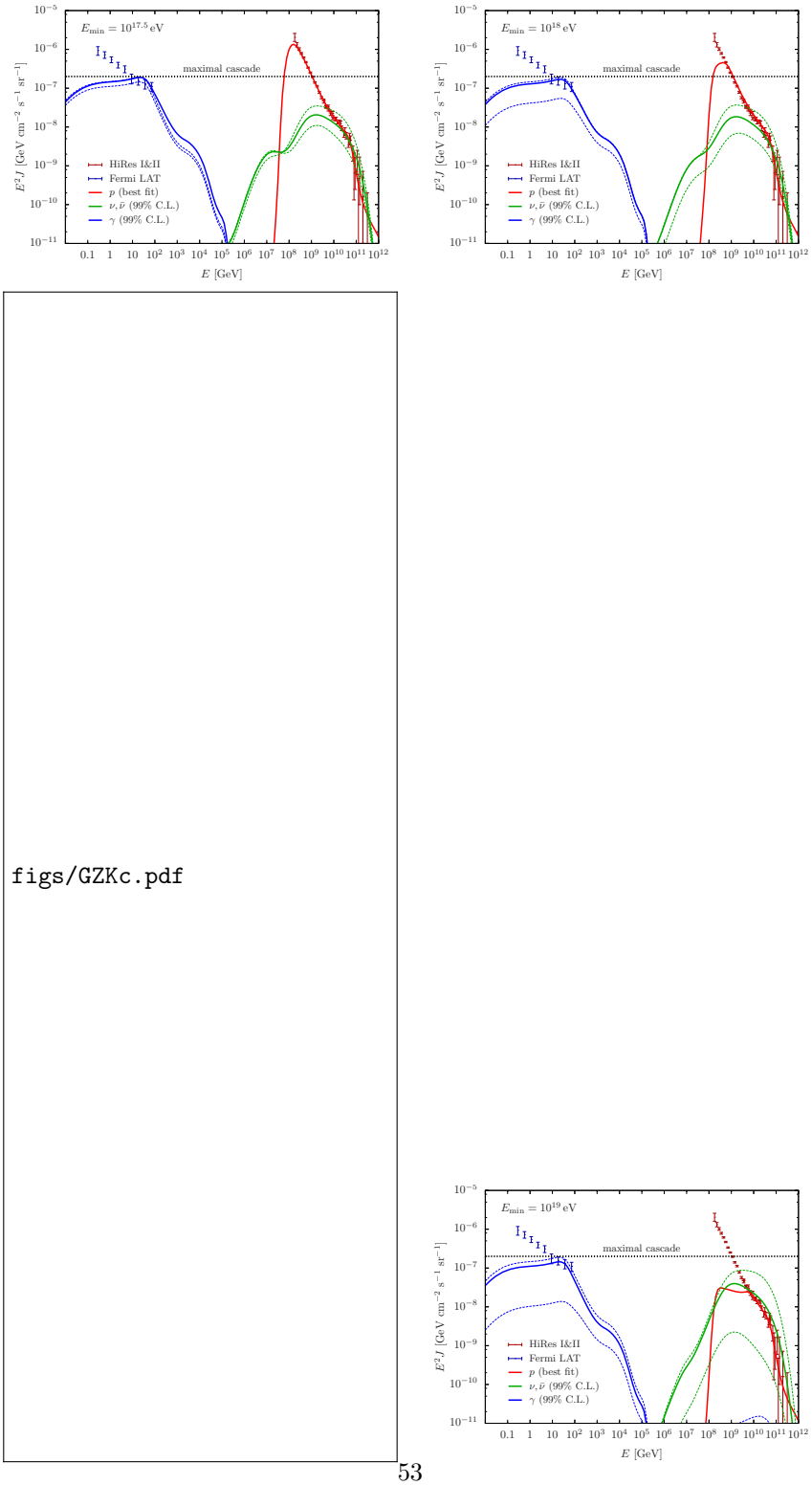

figs/GZKc.pdf

Figure 10: Comparison of proton, neutrino, and gamma-ray fluxes produced in interactions on the CMB by cosmic-ray protons, fitted to HiRes data. We repeat the calculation for four values of the crossover energy, marking the transition to the extragalactic cosmic-ray flux. We show the best-fit values (solid lines) as well as neutrino and gamma-ray fluxes within the 99% C.L. with minimal and maximal energy density (dashed lines). The gamma-ray fluxes are marginally

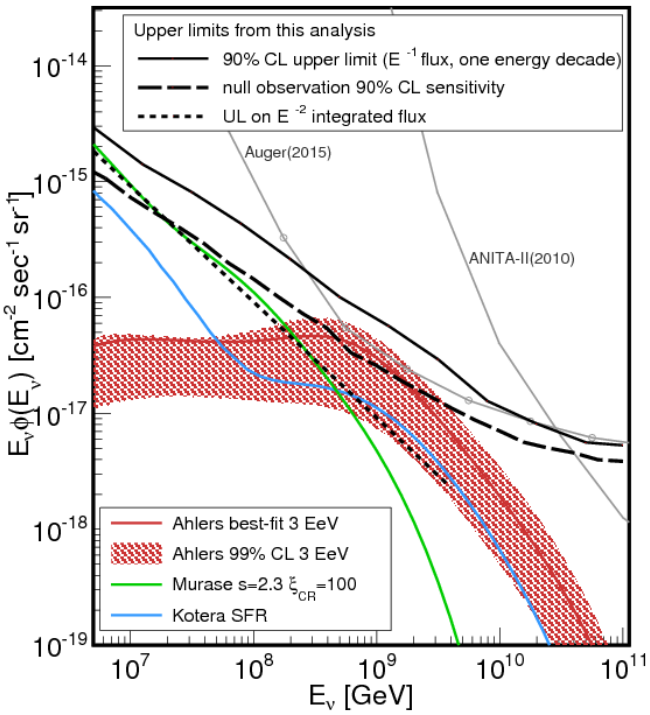

Figure 11: All-flavor-sum of the GZK neutrino flux quasi-differential 90%-CL upper limit on one energy decade E^{-1} flux windows (solid line). The limits are derived using a log-likelihood ratio method. The median null observation limit (sensitivity) is also shown (dashed line). Cosmogenic-neutrino model predictions (assuming primary protons) are shown for comparison: Kotera et al. [73], Ahlers et al. [69], and an astrophysical neutrino model from Murase et al. [74]. Model-independent differential limits on one energy decade E^{-1} flux from Auger [75] and ANITA-II [76] with appropriate normalization are also shown. A model-dependent upper limit on an unbroken E^{-2} power-law flux from the current analysis is shown for reference (dotted line).

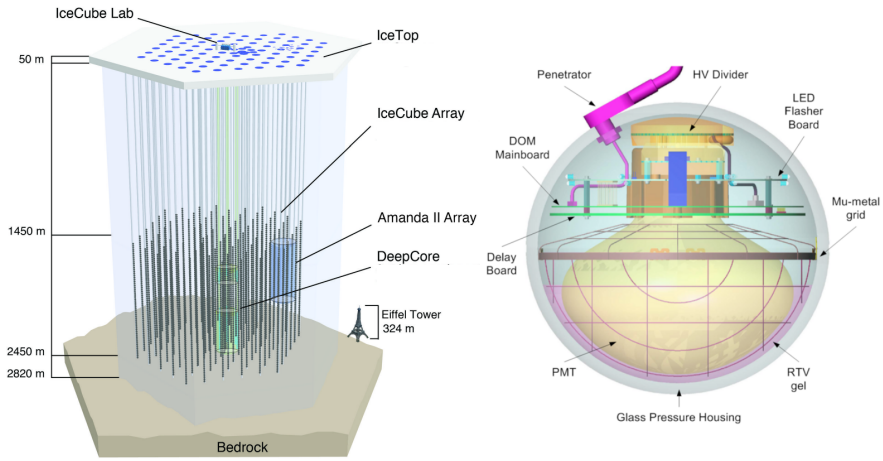

Figure 12: Sketch of the IceCube observatory (left) and the digital optical module (right).

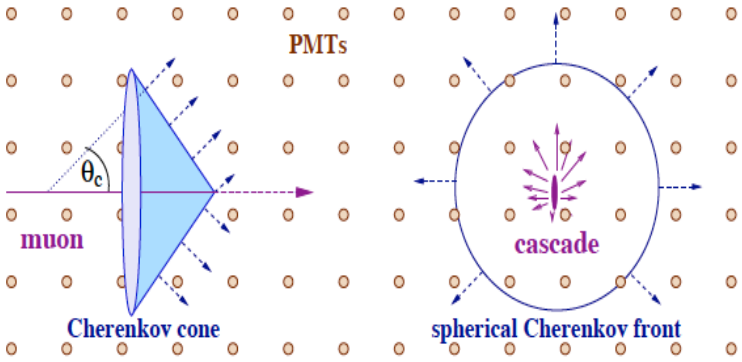

Figure 13: Contrasting Cherenkov light patterns produced by muons (left) and by showers initiated by electron and tau neutrinos (right) and by neutral current interactions. The patterns are routinely referred to as tracks and cascades (or showers). Cascades are produced by the radiation of particle showers, whose dimensions are in the tens of meters, i.e., an approximate point source of light with respect to the dimensions of the detector.

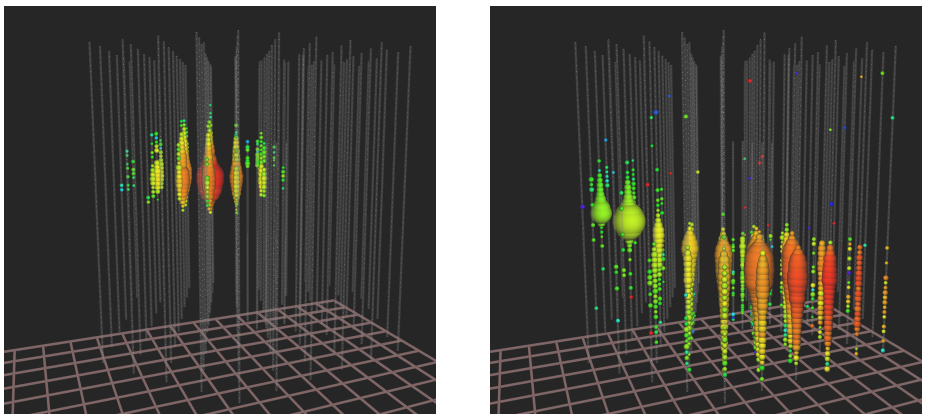

Figure 14: Light pools produced in IceCube by neutrino interactions. White dots represent sensors with no signal. For the colored dots, the color indicates arrival time, from red (early) to purple (late) following the rainbow, and size reflects the number of photons detected. Left: A shower initiated by an electron or a tau neutrino or by the neutral current interaction of a neutrino of any of the three flavors. The measured energy of the shower is 1.14 PeV, which represents a lower limit on the energy of the neutrino that initiated the shower. Right: An upgoing muon track traverses the detector at an angle of 11° below the horizon. The deposited energy inside the detector is 2.6 PeV.

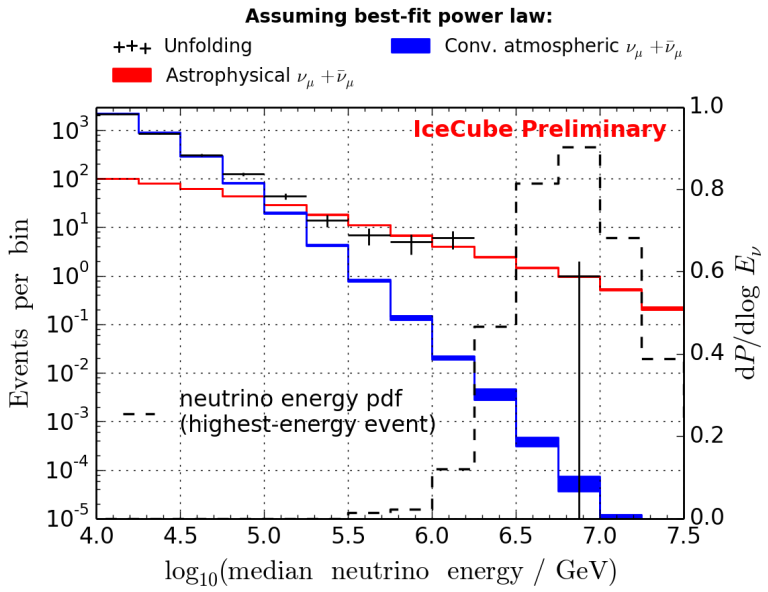

Figure 15: Spectrum of secondary muons initiated by muon neutrinos that have traversed the Earth, i.e., with zenith angle less than 5° above the horizon, as a function of the energy they deposit inside the detector. For each reconstructed muon energy, the median neutrino energy is calculated assuming the best-fit spectrum. The colored bands (blue/red) show the expectation for the conventional and astrophysical contributions. The black crosses show the measured data. Additionally, the neutrino energy probability density function for the highest energy event assuming the best-fit spectrum is shown (dashed line).

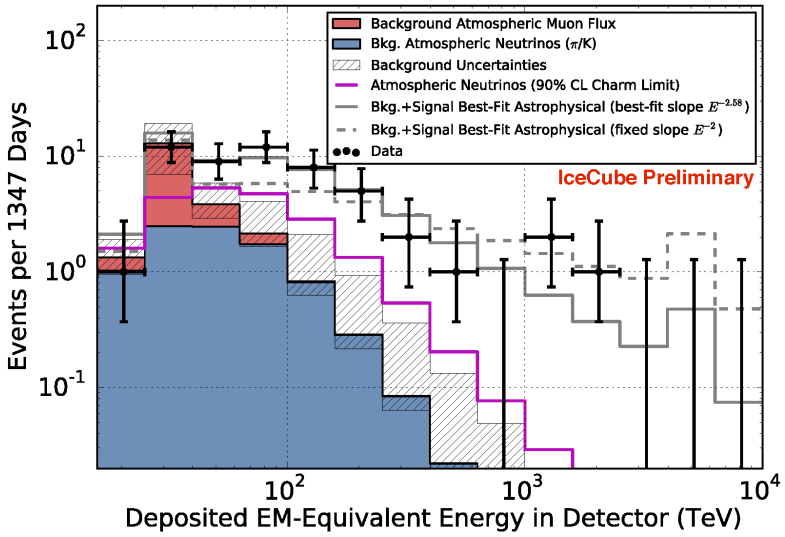

Figure 16: Deposited energies, by neutrinos interacting inside IceCube, observed in four years of data. The hashed region shows uncertainties on the sum of all backgrounds. The atmospheric muon flux (red) and its uncertainty is computed from simulation to overcome statistical limitations in our background measurement and scaled to match the total measured background rate. The atmospheric neutrino flux is derived from previous measurements of both the π, K, and charm components of the atmospheric spectrum [100]. Also shown are two illustrative power-law fits to the spectrum.

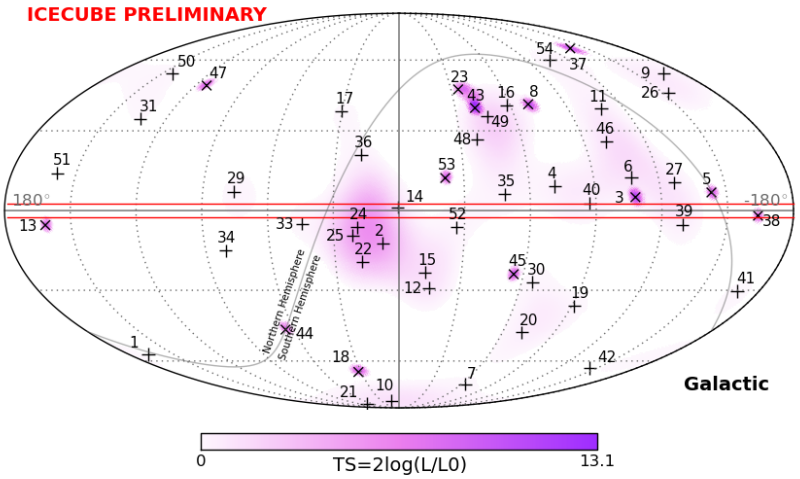

Figure 17: Arrival directions of neutrinos in the four-year starting-event sample in Galactic coordinates. Shower-like events are shown with "+" and those containing muon tracks with "×." The color scale indicates the value of the test statistic (TS) of an unbinned maximum likelihood test searching for anisotropies of the event arrival directions. The horizontal red lines indicate the minimum width (and step size) of ±2.5° used in the search for extended emission along the Galactic plane. Note that the track-like event 28 has been omitted following the discussion in Ref. [101].

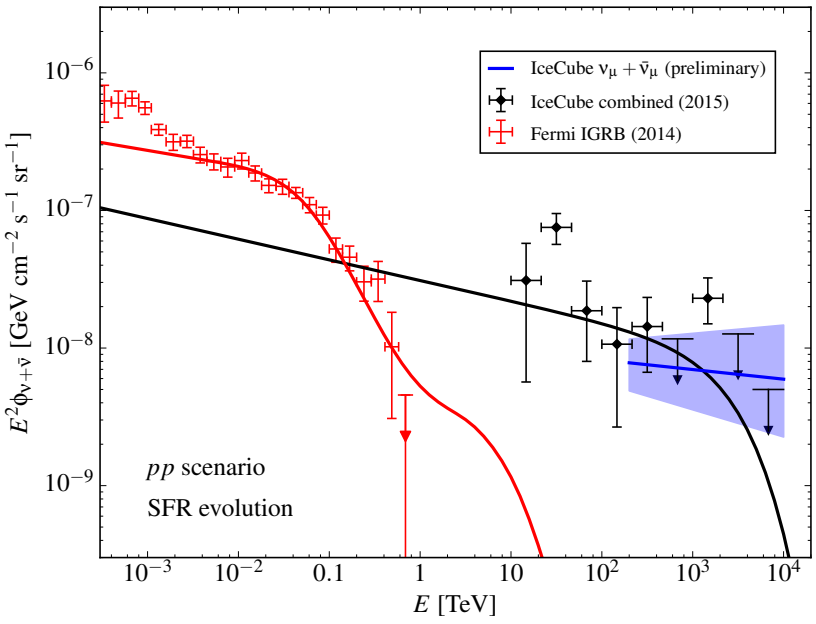

Figure 18: The figure shows that the astrophysical neutrino flux (black line) observed by IceCube matches the corresponding cascaded gamma-ray flux (red line) observed by Fermi. We here assume that the decay products of neutral and charged pions from *pp* interactions are responsible for the nonthermal emission in the Universe [106]. The black data points are combined IceCube results, including the three-year "high-energy starting event" (HESE) analysis [101] and a subsequent analysis lowering the energy threshold for events starting in the detector even further [104]. Also shown is the best fit to the flux of high-energy muon neutrinos penetrating the Earth.

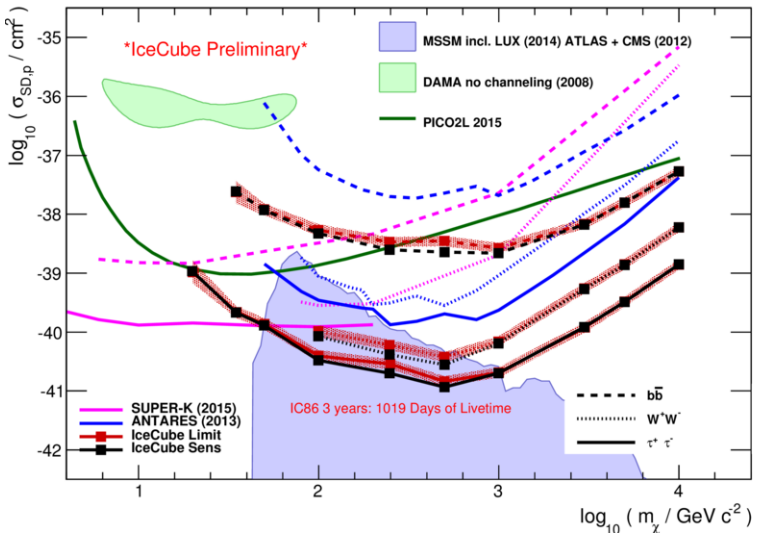

Figure 19: Upper limits at 90% confidence level on the spin-dependent neutralino-proton cross section assuming that the neutrinos are produced by $b\bar{b}, \tau\bar{\tau}$, and W^+W^- annihilation. Limits from IceCube [120, 124, 125], Super-K [128], and ANTARES [129] are shown. Full lines refer to limits on the annihilation channel and dashed lines to the $b\bar{b}$ channel. Direct search results from PICO [130] and tentative signal regions [131, 132, 133] (green-shaded area) are included for comparison. The purple-shaded region indicates the allowed parameter space in MSSM supersymmetric dark matter models that are not ruled out by other experiments.

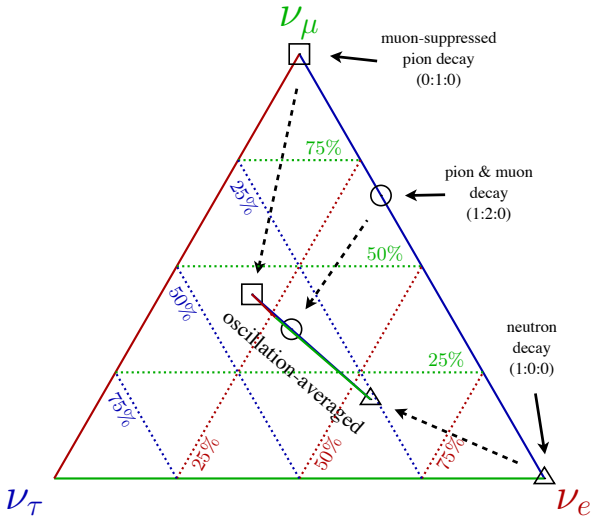

Figure 20: Neutrino flavor phase space after oscillation. We use the best-fit oscillation parameters $\sin^2\theta_{12} = 0.304$, $\sin^2\theta_{23} = 0.577$, $\sin^2\theta_{13} = 0.0219$, and $\delta = 251^\circ$ following Ref. [154] updated after *Neutrino 2014*. Each position in the triangle parametrizes a general initial flavor ratio $(\nu_e : \nu_\mu : \nu_\tau)$. We also indicate specific ratios for neutron decay and pion production. The inner triangle is the corresponding observable phase space after decoherence of the neutrino flavor state over large times or distances.

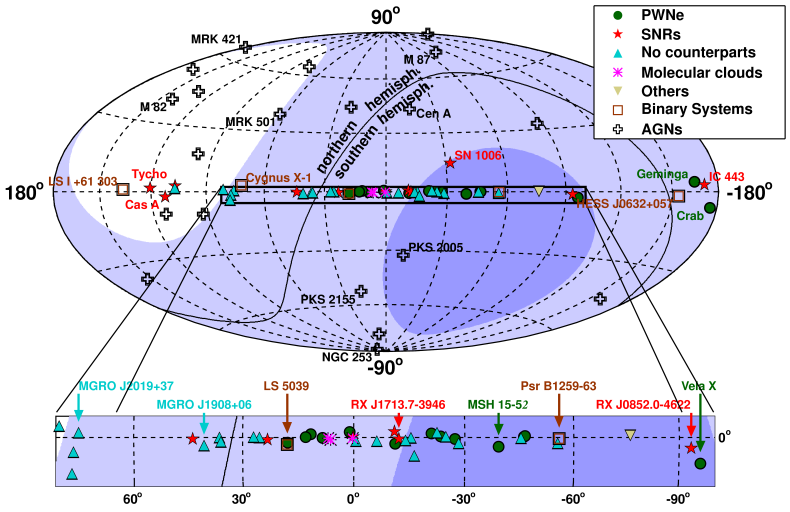

Figure 21: Field of view of IceCube (i.e., the Northern Hemisphere) and of a Mediterranean-based neutrino telescope in Galactic coordinates. Downward sensitivity of 2π is assumed. Shades of blue indicate the fraction of time sources are visible for the northern telescope (light blue: $> 25\%$ of the time; dark blue: $> 75\%$ of the time). Also indicated are sources of high-energy gamma rays, i.e., candidates for neutrino emission. Figure courtesy of A. Kappes.

Figure 22: Prototype of a multi-photomultiplier optical module for KM3NeT. The module incorporates 31 3-inch photomultipliers, their high-voltage bases, and the electronic modules for signal digitization and communication to shore. Photograph by KM3NeT Collaboration.